



Bi-objective motion trajectory generation and online modification of a large rotary crane considering load-sway suppression and collision avoidance

Abdallah Farrage ^{a,b}*, Min Set Paing ^b, Nur Azizah Amir ^b, Hideki Takahashi ^c, Shintaro Sasai ^c, Hitoshi Sakurai ^c, Masaki Okubo ^c, Naoki Uchiyama ^b

^a Mechatronics Engineering Department, Faculty of Engineering, Assiut University, Assiut 71516, Egypt

^b Department of Mechanical Engineering, Toyohashi University of Technology, Toyohashi, 441-8580, Japan

^c Kobelco Construction Machinery Co., Ltd., Hiroshima, 731-5161, Japan



ARTICLE INFO

Communicated by X. Jing

Keywords:

Large rotary crane
Load-sway suppression
Trajectory generation
Online modification
Optimal control
One-degree-of-freedom

ABSTRACT

The main challenge in the automation of the large rotary crane with tower-torsion is the accurate positioning and vibration suppression of the load-sway. The start-of-the-art optimal trajectory generation approaches need to consider several state and input constraints to increase the accuracy; therefore, it requires a large amount of computation time and is not applicable for the practical environment. This study presents an efficient method for optimal trajectory generation considering load-sway suppression and collision avoidance in a fast computation time, which includes two control strategies: the offline bi-objective trajectory generation between the contradictory objectives of total motion time and the collision avoidance fitting function, and the online modification of the optimal trajectory, which is formulated as one-degree-of-freedom optimization to reduce the total motion time and satisfy the entire constraints. The experimental validation with a lab-scale three-dimensional rotary crane is provided to show the effectiveness of the proposed method for practical applications.

1. Introduction

Large rotary cranes play an important role in the construction and manufacturing industries such as ports-and-harbors, nuclear or petrochemical plants, bridge, railways, and many other industrial applications due to their mobility and ability of handling large and heavy items [1,2]. The crane mainly consists of a lower traveling body, an upper turning body, a counter weight, a tower boom, and a jib. The crane movement is described in the horizontal and vertical directions with respect to the ground, which consists of three main motions: slewing, luffing, and hoisting as shown in Fig. 1. The payload is generally suspended from the tip of the structure by a flexible rope to be able to reach a large attitude in position as a benefit over any other lifting machines. As a trade-off, the crane produces a two-dimensional (2D) spherical-like load sway motion when it moves from one place to another. Generally, large cranes are supported with latticed boom structures, which are the main components of lifting heavy-loads and their self weights. The lattice boom structures have the high rigidity in the compression and low rigidity in torsional direction, which lead to the tower-torsion, adding the oscillations in the horizontal turning direction [3].

According to the study in [4], around 43% of crane accidents are caused by the failure of the crane operator's responsibilities; therefore, the safety of the manual driving is greatly dependent on the human operator's skill. Uncontrolled movement of the crane

* Corresponding author at: Mechatronics Engineering Department, Faculty of Engineering, Assiut University, Assiut 71516, Egypt.
E-mail addresses: abdallahfraag@aun.edu.eg (A. Farrage), uchiyama@tut.jp (N. Uchiyama).

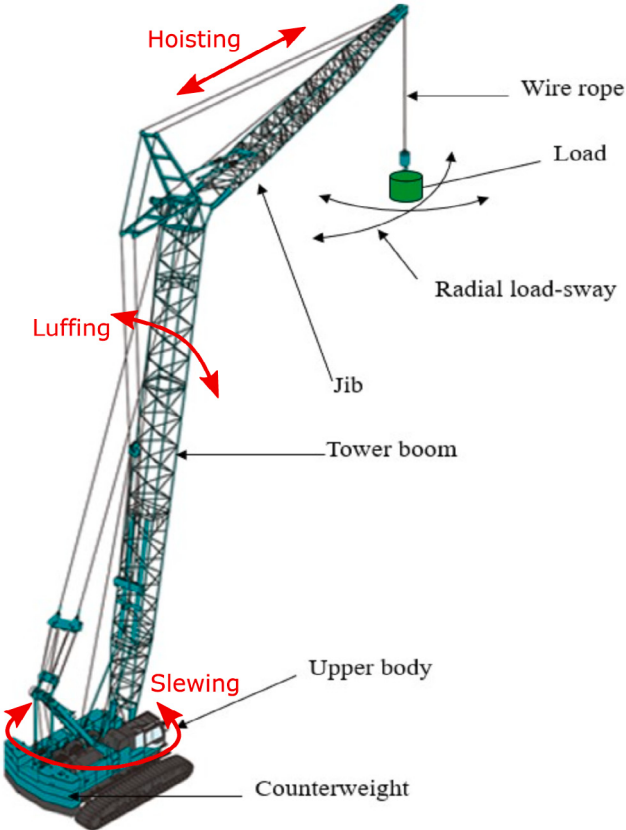


Fig. 1. A three-dimensional rotary crane.

may generate large vibrations of the load-sway, which can be hazardous for human workers and nearby structures, as well as increase the cycle time and reduce working efficiency. Automation is one of the most popular topic in the industrial sector to increase the performance of the industrial machines and to reduce the human-related error. Especially for the crane operation, the main target is to move/transfer the loads in an optimal motion time, without colliding the obstacles. Therefore, the problem formulation of the optimal movement of the load from the start to the target position considering the kinematics and dynamic limitations of the crane, including the obstacle avoidance and load-sway minimization becomes an important process in the literature.

Control strategies on gantry (overhead) cranes are extensively studied for decades; for instance, sliding mode control [5,6], adaptive coupling control [7], and gain feedback scheduling [8,9], and an adaptive full-state controller for under-actuated systems to achieve error elimination and satisfy state constraints [10]. Moreover, Yang et al. introduced precise motion control and adherence to full-state constraints by proposing an adaptive output-feedback controller without using exact system models or velocity feedback. Additionally, all of state variables remain within predefined time-variant ranges and eventually converge to their desired values [11]. Furthermore, open-loop controls such as input shaping [12,13], whereas a few pay attention to the rotary crane boom control. A partial feedback gain is provided for rotary cranes that provides a robust stability with respect to any rope length in [14]. The crane systems subjected to internal and external disturbances that amplify load sway are controlled using an observer-based proportional controller. The observer was designed to compensate for disturbances, while the proportional controller ensures the asymptotic stability. The integration of a controller and an observer enables the crane to follow a desired reference trajectory effectively while minimizing load sway [15]. A linear feedback controller is implemented by linearizing and decoupling the complex non-linear model of rotary crane [16]. The residual skew vibration of the payload is successfully reduced by applying a robust sliding mode controller in [17]. However, Neupert et al. [18] highlighted that only a limited number of control strategies were demonstrated to contribute in practical applications. This limitation is attributed to challenges such as accurately measuring load sway and addressing parameter variations. Moreover, implementing such control approaches in existing large crane systems on-site is challenging, as they require modifications of the crane's hardware components.

Due to the aforementioned limitations, two-steps control approach is normally considered in the literature for the practical usage: the feedforward planning of the reference trajectory considering the obstacle avoidance scheme and system limitations, and the accurate tracking of the reference trajectory by the feedback controller. This paper focuses on the former step because the latter requires the installation of additional sensors and the implementation of new feedback controllers guaranteeing the safe and

stable operations against unknown disturbances and happenings. The differential flatness approaches in [19,20] also perform as a feedforward control of the machine which linearizes the non-linear system by parameterizing the system states and inputs. However, constraints on the system states and inputs are often neglected or not satisfied due to the mapping between the flat output and the nonlinear system. Another simple and effective approach is the optimal trajectory generation, where all the states and inputs are allowed as constraints to formulate the optimal control program (hereafter OCP) using nonlinear programming techniques.

Coupled approaches in which the obstacle avoidance or the geometric constraints are generally included in the optimal trajectory generation [21]. On the other hand in decoupled approaches, the optimal control scheme is separated into the obstacle avoidance path planning using the higher level path planners (e.g., A* algorithm to generate the shortest distance from the start to goal without collision [22]), and the optimal trajectory generation to minimize the specific objective (e.g., the total motion time [23–25] and smoothness or dynamic criteria [26]). In this case, the obstacle avoidance scheme usually takes part as an additional objective function, which acts as a soft constraint in the problem formulation. Weight scheduling is one of the most common method to solve the multi-objective OCPs by multiplying with corresponding weights to each objective, then sums up all to form an aggregated scalar objective function [27]. Since the nature of objective functions are different to each other, it is challenging to determine the corresponding weights for achieving a specific trade-off. Moreover, the abovementioned OCPs are generally solved by the state-of-the-art direct transcription method [28] where all the states and inputs are discretized first and the OCP is solved by the nonlinear programming methods. To guarantee the accuracy of the constraints, several discrete points (grids) are taken into account in an OCP; therefore, the computational complexity becomes very high to be used in online applications.

For this reason, the OCPs are solved offline first to generate an optimal motion trajectory considering several constraints and the online modification of an optimal trajectory is implemented thereafter. In [29], a robotic manipulator working in a rectangular space, whose modified positions are generated online by scaling of an optimal trajectory. Although, the computation time is very small, this method does not allow constraints nor objectives for trajectory modification; therefore, it is limited only for small positioning changes. In [30], an anti-sway component is introduced to the smooth reference trajectory for accurate positioning of an overhead crane in real-time. The offline optimal trajectories are stored in a database and small deviations from the closest trajectory are computed as solutions of a linear constrained quadratic programming [31]. The experimental validation is included with a lab-scale three-dimensional (3D) gantry crane in [32]. According to the best of author's knowledge, the 3D optimal trajectory generation of the rotary crane considering a specific trade-off between contradictory objectives and its real-time modifications with respect to the moving targets are not fully investigated.

This paper extends the previous simulation [33] that conducts the offline optimal trajectory generation and modifies it online only by the horizontal boom movement. In the previous study [33], weighting factors for optimization do not consider the trade-off of the contradictory objectives. Thereafter, the online of modification neglects the obstacle information available. In this paper, the offline trade-off solutions between the two contradictory objectives: the total motion time and the least square fitting function for avoiding the obstacle, are presented by changing the normalized normal constraint method (NNC) [34]. Furthermore, the online modifications of the original optimal trajectory, which can be achieved by slightly shifting the target positions away from their original locations, are implemented considering the same predefined obstacles from the original optimization as additional constraints. The motion is parameterized by one of the novel multi-point trajectories in robotic applications (refer to [35] for details): cubic B-splines for the smoothness and the continuity up to acceleration. B-splines are also effective for real-time modification due to their local modification property; therefore, it avoids computation of the entire trajectory. The nonlinear OCP is solved by the sequential quadratic programming (SQP) [36]. According to the on-line modification of the optimal trajectory, the modification approach presented in [29] is highly suitable for online adjustments because it requires minimal computational time. Therefore, the above modifying approach has been used as a benchmark for comparison with the modification approach in this study. Moreover, the proposed trajectory is initially estimated based on the utilization of a scaling factor (SF). In order to satisfy the constraints, we consider modifying each degree-of-freedom (i.e., horizontal and vertical boom angles, and the rope length) with respect to the total motion time. As a result of reducing optimization variables, the computation time decreases proportionally, and the solution satisfies load-sway and actuator constraints in online applications. Comparative studies for trajectory modification: horizontal and vertical boom angles, rope length, comparing with the SF are analyzed in terms of the total motion time, obstacle avoidance scheme, and the computation time. The simulation results are validated with a lab-scale 3D rotary crane system, in which all motions of the boom, rope length, and sway-angles are measured by the indoor motion capture system.

The rest of the paper is organized as follows: Section 2 briefly states the crane dynamics, obstacle avoidance scheme, control objectives, and constraints to formulate the general OCP; followed by reformulation of the problem by a smooth parameterization in terms of cubic B-splines in Section 3; Section 4 represents the offline formulation of the bi-objective optimization problem utilizing the NNC and SQP methods; the online trajectory generation method is presented in Section 5; simulation results of both offline and online optimal trajectory generations are compared in Section 6; the experimental validations with our laboratory crane are included in Section 7; and the conclusions and future works are described in Section 8. Appendix includes the pseudo-codes for the proposed algorithms, involving bi-objective optimization and online modifications steps.

2. Crane dynamics, obstacle avoidance, and control objectives

2.1. Crane dynamics with tower-torsion

This study aims to generate an optimal motion trajectory of the rotary crane considering the total motion time, obstacle avoidance, dynamics, and kinematic constraints, and to modify the optimal trajectory in a small computational time without

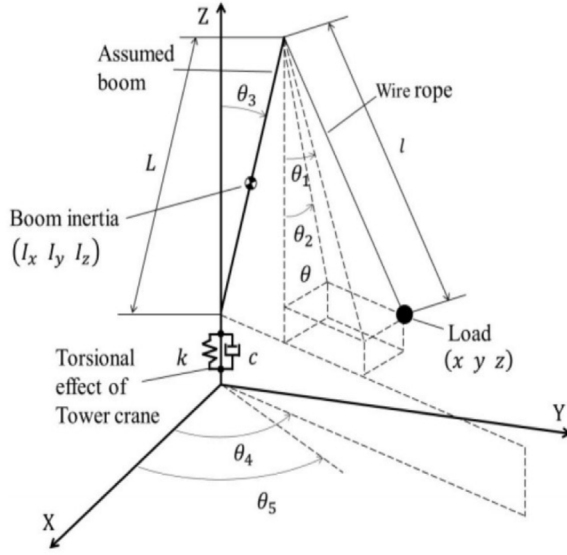


Fig. 2. Schematic representation of a rotary crane system with tower-torsion.

violating the constraints. In this study, we consider the simplified model of a rotary crane in [3], in which the tower boom and the jib are considered as a straight-line body as shown in Fig. 2. The assumed boom with a constant length L rotates in the vertical and horizontal directions by the actuator angles θ_3 and θ_5 , respectively. The spring damper characteristics are added to the turning direction of the horizontal boom angle, which results the new horizontal angle due to the boom-twisting effect denoted by θ_4 , and the load is suspended from the tip of the boom by a variable rope length l . Therefore, the following load-sway dynamics, in which the model verification was conducted in [37], is used to generate an optimal motion trajectory as follows:

$$\begin{aligned} & I(l + l\theta_1^2)\ddot{\theta}_1 + l\dot{l}(2\dot{\theta}_1 - 2\theta_2\dot{\theta}_4 + 2\theta_1^2\dot{\theta}_1 + 2\theta_1\theta_2\dot{\theta}_2) + l^2(-\theta_2\ddot{\theta}_4 - 2\dot{\theta}_2\dot{\theta}_4 - \theta_1\dot{\theta}_4^2 + \theta_1\dot{\theta}_1^2 + \theta_1\dot{\theta}_2^2) + Ll(\ddot{\theta}_3 \cos \theta_3 - \\ & \theta_3^2 \sin \theta_3 - \theta_1\dot{\theta}_3 \sin \theta_3 - \theta_1\dot{\theta}_3^2 \cos \theta_3 - \dot{\theta}_4^2 \sin \theta_3) + L\dot{l} \sin \theta_3 (-\theta_1\dot{\theta}_3 + \dot{\theta}_3) + g\dot{l}\theta_1 = 0, \\ & I(l + l\theta_2^2)\ddot{\theta}_2 + l\dot{l}(2\dot{\theta}_2 - 2\theta_1\dot{\theta}_4 + 2\theta_2^2\dot{\theta}_2 + 2\theta_1\theta_2\dot{\theta}_1) + l^2(\theta_1\ddot{\theta}_4 + 2\dot{\theta}_1\dot{\theta}_4 - \theta_2\dot{\theta}_4^2 + \theta_2\dot{\theta}_2^2 + \theta_2\dot{\theta}_1^2) + Ll(\ddot{\theta}_4 \sin \theta_3 + \\ & 2\dot{\theta}_3\dot{\theta}_4 \cos \theta_3 - \theta_2\dot{\theta}_3^2 \cos \theta_3 - \theta_2\dot{\theta}_3 \sin \theta_3) - 0.5\dot{l}^2\theta_2 + g\dot{l}\theta_2 = 0, \\ & I(\ddot{\theta}_5 - \dot{\theta}_4) + c(\dot{\theta}_5 - \dot{\theta}_4) + k(\theta_5 - \theta_4) = 0, \end{aligned} \quad (1)$$

where I and g are the boom inertia and the gravitational acceleration, and k and c are the spring and damping coefficients of the crane system, respectively. The simultaneous movement of the horizontal and vertical boom angles and the wire length generates the two-dimensional (2D) load sway: θ_1 and θ_2 , which move in radial and tangential direction to the horizontal boom motion, respectively.

2.2. Obstacle avoidance path generation in joint space

Given a start and target point in the Cartesian coordinate frame, a collision-free path is generated in terms of via-points. This study employs the A* algorithm, which is simple and effective for avoiding the obstacles by calculating the heuristic value at each node and expanding the nodes until it reaches the target [38]. For the crane system, the algorithm generates a set of via-points based on the shortest distance traveled for the horizontal and vertical boom angles, and the wire length. For details, refer to the authors' work for a large rotary crane system in [37].

A collision-free position $\chi^* = [x^*, y^*, z^*]^T$ at the Cartesian coordinate frame is represented by

$$\begin{aligned} x^* &= L \sin \theta_3^* \cos \theta_5^* - l^* \theta_1^* \cos \theta_5^* - l^* \theta_2^* \sin \theta_5^*, \\ y^* &= L \sin \theta_3^* \sin \theta_5^* + l^* \theta_1^* \sin \theta_5^* + l^* \theta_2^* \cos \theta_5^*, \\ z^* &= L \cos \theta_3^* - l^* \cos \sqrt{\theta_1^{*2} + \theta_2^{*2}}. \end{aligned} \quad (2)$$

This study considers motion trajectory generation in the joint space of the actuators. Given positions at the Cartesian coordinate frame, the following inverse kinematics is used to transform the respective reference via-point $\boldsymbol{\Theta}^* = [\theta_3^*, \theta_5^*, l^*]^T$ as follows:

$$\begin{aligned}\theta_3^* &= \sin^{-1} \left[\sqrt{\frac{x^{*2} + y^{*2}}{L^2}} \right], \\ \theta_5^* &= \cos^{-1} \left[\frac{x^*}{L \sin \theta_3^*} \right], \\ l^* &= L \cos \theta_3^* - z^*.\end{aligned}\tag{3}$$

For simplicity, Eqs. (2) and (3) are considered as the ideal cases (i.e., the sway angles θ_1^* and θ_2^* are assumed zeros), and the boom twist is considered negligible (i.e., the horizontal boom angles θ_4^* and θ_5^* are considered as equivalent) in the initial path generation. Thereafter, the OCP for generating an optimal trajectory is stated by considering kinematic and dynamic properties of the crane, including the load-sway limits in Section 2.3.

2.3. Control objectives and constraints

For allowing the smooth transitions at the start and end of the trajectory, the initial and final velocities and accelerations must be zero, satisfying the start and target load-positions. Therefore, the following conditions are added as equality constraints to the problem formulation:

$$\begin{aligned}\boldsymbol{\Theta}(0) &= \boldsymbol{q}_0, \quad \dot{\boldsymbol{\Theta}}(t_f) = \boldsymbol{q}_f, \\ \dot{\boldsymbol{\Theta}}(0) &= \mathbf{0}, \quad \ddot{\boldsymbol{\Theta}}(t_f) = \mathbf{0}, \\ \ddot{\boldsymbol{\Theta}}(0) &= \mathbf{0}, \quad \dddot{\boldsymbol{\Theta}}(t_f) = \mathbf{0},\end{aligned}\tag{4}$$

where $\boldsymbol{\Theta} = [\theta_3, \theta_5, l]^T$ represents the position vector, and $\dot{\boldsymbol{\Theta}}$ and $\ddot{\boldsymbol{\Theta}}$ are the velocity and acceleration vectors with respect to the time $t \in [0, t_f]$, where t_f is the total motion time. The symbols \boldsymbol{q}_0 and \boldsymbol{q}_f are denoted as the start and target load-positions. In order to avoid the extremities of actuator positions and velocities, the inequality constraints are considered along the motion trajectory as follows:

$$\begin{aligned}q_{\min} &\leq \boldsymbol{\Theta}(t) \leq q_{\max}, \\ \dot{q}_{\min} &\leq \dot{\boldsymbol{\Theta}}(t) \leq \dot{q}_{\max},\end{aligned}\tag{5}$$

where q_{\min} and q_{\max} are the upper and lower bounds of the actuator positions, and \dot{q}_{\min} and \dot{q}_{\max} are the upper and lower bounds of the actuator velocities, respectively. The limitation of the above constraints in Eq. (5) plays an important role for optimizing the sway angles $\boldsymbol{\Psi} = [\theta_1, \theta_2]^T$ and their respective velocities $\dot{\boldsymbol{\Psi}} = [\dot{\theta}_1, \dot{\theta}_2]^T$ along the motion, which must be bounded by

$$\begin{aligned}\rho_{\min} &\leq \boldsymbol{\Psi}(t) \leq \rho_{\max}, \\ \dot{\rho}_{\min} &\leq \dot{\boldsymbol{\Psi}}(t) \leq \dot{\rho}_{\max},\end{aligned}\tag{6}$$

where ρ_{\min} , $\dot{\rho}_{\min}$, ρ_{\max} , and $\dot{\rho}_{\max}$ are the upper and lower bounds of load-sway angular positions and velocities, respectively. Besides, the abovementioned load-sway conditions should be suppressed as much as possible when the load reaches the target at time t_f ; therefore, the additional constraints are added to the problem as follows:

$$\begin{aligned}\rho_{f\min} &\leq \boldsymbol{\Psi}(t_f) \leq \rho_{f\max}, \\ \dot{\rho}_{f\min} &\leq \dot{\boldsymbol{\Psi}}(t_f) \leq \dot{\rho}_{f\max},\end{aligned}\tag{7}$$

where $\boldsymbol{\Psi}(t_f)$ and $\dot{\boldsymbol{\Psi}}(t_f)$ represent the final load-sway position and velocity, $\rho_{f\min}$, $\dot{\rho}_{f\min}$, $\rho_{f\max}$, and $\dot{\rho}_{f\max}$ are the upper and lower limits of the final load-sway positions and velocities, respectively. Finally, the total motion time must be always greater than zero, which is described as follows:

$$t_f > 0.\tag{8}$$

In this study, we consider the following two objectives from our previous study [33]: the total motion time for enhancing the productivity and the least square fitting function for satisfying the obstacle avoidance scheme by the A* algorithm. Minimizing the position difference between the generated trajectory and A* via-points acts as a soft constraint for avoiding the obstacle. On the other hand, it increases the total motion time due to its contradictory nature. Assume N^{th} discrete via-points $\boldsymbol{\chi}_k^* = [x_k^*, y_k^*, z_k^*]^T$, $k = \{0, 1, \dots, N\}$ at the Cartesian coordinate frame, the respective transformations $\boldsymbol{\Theta}_k^* = [\theta_{3k}^*, \theta_{4k}^*, l_k^*]^T$ are generated by the inverse kinematics in Eq. (3). In this case, the nonlinear OCP is stated as follows:

$$\min_{\phi} \{F_1, F_2\},\tag{9}$$

with

$$\begin{aligned}F_1 &= t_f, \\ F_2 &= \|\boldsymbol{\Theta}(t_k) - \boldsymbol{\Theta}_k^*\|_2^2, \quad k = \{0, 1, \dots, N\}, \\ \phi &= \{t_f, \boldsymbol{\Theta}(\cdot)\},\end{aligned}\tag{10}$$

subject to Eqs. (4)–(8).

The notation $\|\cdot\|_2$ is the Euclidean norm.

3. Parameterization of a motion trajectory

In this section, the parameterization method of a motion trajectory is discussed before the OCP reformulation. In order to generate a smooth motion, the continuity in at least acceleration of the trajectory must be guaranteed. For this reason, this study uses the cubic B-spline (order $r = 4$) with $(m + 1)$ control points to represent the trajectory. The advantage of using B-splines than any other parameterization methods (e.g., a polynomial function) is the local modification property and the flexibility of increasing/decreasing of control points independently from the order of B-splines. The motion trajectory is defined as follows:

$$\mathbf{s}(u) = \sum_{j=0}^m B_{j,r}(u) \mathbf{c}_j, \quad \forall u \in [0, 1], \quad (11)$$

where $\mathbf{s}(u) = [\theta_3(u), \theta_5(u), l(u)]^T$ defines the load-position vector with a dimensionless parameter u ranging from 0 to 1, $B_{j,r}(u)$ is the basis function, and \mathbf{c}_j represents the control vector of B-spline. The knot vector has a uniform distribution, which is repeated at the start and end of the trajectory for r -times as follows:

$$\mathbf{u} = [\underbrace{0, \dots, 0}_{r\text{-times}}, \underbrace{u_1, u_2, \dots, u_{m-3}, 1, \dots, 1}_{r\text{-times}}]. \quad (12)$$

The position of the load is represented in the parameter space $u \in [0, 1]$, whereas its time-derivatives are in the time space $t \in [0, t_f]$. Thus, the velocity and acceleration of the trajectory with respect to the motion time t are described as follows:

$$\mathbf{v}(t) = \frac{\dot{\mathbf{s}}(u)}{t_f}, \quad \forall u \in [0, 1], \quad (13)$$

$$\mathbf{a}(t) = \frac{\ddot{\mathbf{s}}(u)}{t_f^2}, \quad (14)$$

with the simple scaling law between the motion time t and the parameter u :

$$u = \frac{t}{t_f}, \quad \forall t \in [0, t_f], t_f > 0, \quad (15)$$

where $\dot{\mathbf{s}}(u)$ and $\ddot{\mathbf{s}}(u)$ are the first and second derivatives with respect to parameter $u \in [0, 1]$, respectively. The OCP statement in terms of cubic B-spline is defined as follows:

$$\min_{\phi} \{F_1, F_2\}, \quad (16)$$

with

$$\begin{aligned} F_1 &= t_f, \\ F_2 &= \|\mathbf{s}(u_k) - \boldsymbol{\Theta}_k^*\|_2^2, \quad k = \{0, 1, \dots, N\}, \\ \boldsymbol{\phi} &= \{t_f, \mathbf{c}_0, \mathbf{c}_1, \dots, \mathbf{c}_m\}, \end{aligned} \quad (17)$$

subject to

$$\begin{aligned} \mathbf{s}(0) &= \mathbf{q}_0, \mathbf{s}(0) = \mathbf{q}_f, \\ \mathbf{v}(0) &= \mathbf{0}, \mathbf{v}(t_f) = \mathbf{0}, \\ \mathbf{a}(0) &= \mathbf{0}, \mathbf{a}(t_f) = \mathbf{0}, \end{aligned} \quad (18)$$

$$q_{\min} \leq s(u) \leq q_{\max}, \quad (19)$$

$$\dot{q}_{\min} \leq v(t) \leq \dot{q}_{\max}, \quad (20)$$

$$\rho_{\min} \leq \Psi(t) \leq \rho_{\max}, \quad (21)$$

$$\dot{\rho}_{\min} \leq \dot{\Psi}(t) \leq \dot{\rho}_{\max}, \quad (22)$$

$$t_f > 0.$$

By using B-spline as the parameterization function, we can consider t_f and control points for each DOF motion as the inputs, $\mathbf{v}(t)$ and $\mathbf{a}(t)$ are the state trajectories, the load-sway and tower-torsion results are the outputs of the crane system.

4. Bi-objective optimization

The OCPs mentioned in Section 3 is bi-objective optimization problem between the two contradictory objectives: the total motion time and the least square fitting function. For instance, the generated trajectory with the most-fitted least square function leads

control points of the B-spline closer to the A* via-points. As a trade-off, the motion time increases to satisfy the equality and inequality constraints in Eqs. (18)–(22). Here, we implement the NNC method, which optimizes one of the objective functions whereas the remaining objective plays as an additional constraint in OCP formulation. As a benefit, the method gives a specific trade-off between contradictory objectives. The extrema of objective sets in Eq. (17) are formulated by minimizing each objective independently as follows:

$$f_{1,\min} = \min_{\phi} F_1, \quad f_{2,\min} = \min_{\phi} F_2, \quad (23)$$

subject to Eqs. (18)–(22).

The solutions in Eq. (23) are mapped into the normalized objective space formulated by

$$\tilde{F}_1 = \frac{F_1 - f_{1,\min}}{f_{1,\max} - f_{1,\min}}, \quad \tilde{F}_2 = \frac{F_2 - f_{2,\min}}{f_{2,\max} - f_{2,\min}}, \quad (24)$$

with

$$\begin{aligned} f_{1,\max} &= t_{\max}, & f_{2,\max} &= F_2(\phi_{1,\min}), \\ \phi_{1,\min} &= \arg \min_{\phi} F_1. \end{aligned} \quad (25)$$

The anchor points \tilde{F}_1^* and \tilde{F}_2^* , which are the extreme coordinates in a normalized plane, can be represented as (0, 1) and (1, 0), respectively by solving Eqs. (24) and (25) independently. Therefore, the optimization problem in Eq. (16) is reformulated as follows by the NNC method:

$$\min_{\phi} \tilde{F}_2, \quad (26)$$

subject to Eqs. (18)–(22), and:

$$n^T [\vartheta - \tilde{F}(\omega)] \leq 0, \quad (27)$$

with

$$\begin{aligned} n &= \tilde{F}_2^* - \tilde{F}_1^* = [1, -1]^T, \\ \vartheta &= [\tilde{F}_1, \quad \tilde{F}_2]^T, \\ \tilde{F}(\omega) &= (1 - \omega)\tilde{F}_1^* + \omega\tilde{F}_2^*, \quad 0 \leq \omega \leq 1, \end{aligned} \quad (28)$$

where $\omega \in [0, 1]$ is the user-specified weighting factor to give solutions with a specified trade-off.

Direct transcription is the most common method to solve the above OCP, which discretizes the problem over the horizon and solves it using conventional nonlinear programming methods (e.g., SQP). Two types of discrete grids are used to solve the OCP: N th grids for fitting the position with A* via-points and n th grids for satisfying velocity and sway constraints. Since the actuator velocity and the load-sway results might violate the constraints between the grids if the constraint accuracy is low (i.e., $n \leq N$). Thus, we assume $n > N$ in this study. Both N th and n th grids are uniformly distributed over the parameter horizon [0, 1].

5. Online trajectory modification

Section 4 describes the reformulation of a spline-based OCP according to the various constraints. Since the trajectory is firstly discretized and then optimized, many grids (discrete-points) are required to be imposed for having a good accuracy of the constraints; therefore, the offline OCP needs a very large computation time. In practice, the relative position change occurs when the crane in motion. Therefore, generating the whole trajectory is not practical for the cases, where the crane operator desires to shift the load position from the original one. For this reason, this section considers the optimal trajectory modifications without entirely recomputing the OCP.

Suppose that it is required to modify the target load-position known as $\chi_f^m = [x_f^m, y_f^m, z_f^m]^T$, which is transformed into the respective coordinates $\Theta_f^m = [\theta_{3f}^m, \theta_{4f}^m, l_f^m]^T$. Assume s^* is the closest trajectory to the modified target and has velocity and acceleration values, v^* and a^* , respectively. Thereafter, the SF is calculated for initializing the trajectory as follows:

$$\alpha = (\Theta_f^m - s^*(0)) \oslash (s^*(1) - s^*(0)), \quad (29)$$

where the operator \oslash represents the element-wise division. The updated control points of B-spline are calculated using the above SF because they are directly proportional to the positions. The initialized control points for modifying the trajectory are determined as follows:

$$c_{j,\text{new}} = \alpha \otimes (c_j - c_0) + c_0, \quad j = \{0, 1, \dots, m\}, \quad (30)$$

where the operator \otimes is the element-wise multiplication. After modifying the control points, the corresponding position, velocity, and acceleration of the trajectory can be calculated using Eqs. (11), (13), and (14). When the start position of the load is required to be changed, we can apply the same approach of SF by shifting the point to the new one without loss of generality. The advantage of using SF for trajectory modification is that it keeps the oscillation property of the original trajectory while small changes occur in position. However, the SF method does not consider any constraints nor objective function; thus the computation time is very small. In this case, the total motion time remains constant and as a drawback, the generated trajectory might fail to satisfy the actuator

limits such as velocity and the dynamic limits such as load-sway. For this reason, we extended an algorithm to modify the optimal trajectory considering both satisfying the constraints and saving the computational effort.

In this study, we use one-degree-of-freedom (1-DOF) control variables and the motion time to modify the optimized trajectory. As explained in Section 4, the motion trajectory is formulated in two spaces: the parameter space for defining the position and the time space for its derivatives. The modified control points in Eq. (30) satisfies the updated start and target positions, velocities, and accelerations due to the properties of B-spline as follows:

$$s^*(0) = c_0, \quad s^*(1) = c_m, \quad (31)$$

$$v^*(0) = \frac{\dot{s}^*(0)}{t_f} = \frac{f(c_0, c_1)}{t_f} = 0, \quad (32)$$

$$v^*(t_f) = \frac{\dot{s}^*(1)}{t_f} = \frac{f(c_{m-1}, c_m)}{t_f} = 0, \quad (32)$$

$$a^*(0) = \frac{\ddot{s}^*(0)}{t_f^2} = \frac{f(c_0, c_1, c_2)}{t_f^2} = 0, \quad (33)$$

$$a^*(t_f) = \frac{\ddot{s}^*(1)}{t_f^2} = \frac{f(c_{m-1}, c_m)}{t_f^2} = 0, \quad (33)$$

where \dot{s}^* and \ddot{s}^* are the first and second derivatives with respect to the parameter u . Since the denominator $t_f > 0$, the numerator functions consisting of the respective control points must be zero to satisfy the null velocities and accelerations in Eqs. (32) and (33). The original OCP has $(m+1)$ variables for each DOF and the total motion time to optimize, summing up to $(3m+4)$ control variables. According to the abovementioned property, we can subtract 18 control variables for the start and end of the motion; therefore, it becomes $(3m - 14)$. Moreover, the original and modified trajectories are assumed similar, we choose to modify only 1-DOF variables (horizontal or vertical boom angle, or rope length) and the total motion time to satisfy the constraints along the trajectory. For this reason, the optimization variables are further reduced to $(m - 4)$ to formulate the problem. The sub-OCP is defined as follows:

$$\min_{\phi} t_f, \quad (34)$$

with

$$\phi = \{t_f, c_{3,\text{new}}, c_{4,\text{new}}, \dots, c_{m-3,\text{new}}\}, \quad (35)$$

subject to the velocity and sway constraints from Eqs. (19)–(22), and the additional position constraint for obstacle avoidance in trajectory modification:

$$|c_{i,\text{new}} - c_i| \leq c_{\text{diff}} \quad (36)$$

where $c_{i,\text{new}}$ and c_i represent the updated and original 1-DOF scalar control points of rotary crane and c_{diff} is user-defined position tolerance for the chosen degree. In other words, control points are polygons of position. Therefore, Eq. (36) imposes the modified DOF trajectory near the original one to avoid obstacles.

6. Simulation

The proposed approach aims to achieve precise crane load positioning with minimal load swaying angles while optimizing motion time without collision. The proposed approach includes two main scenarios: the first one is the offline bi-objective OCP, which is formulated based on the trade-off solutions between the two contradictory objectives: the total motion time and the least square fitting function for avoiding the obstacle. The trade-off scheme is analyzed using NNC and direct transcription methods. The second scenario represents the online modification of the original optimal trajectory without entirely recomputing the OCP to reduce the computational cost. This modification can be achieved by slightly shifting the target positions away from their original locations with considering the same predefined obstacles of the original trajectory to guarantee collision avoidance. The trajectory modification method focuses only on a single degree of freedom motion of the crane, reducing the optimization variables by avoiding the need to solve the entire OCP. Simulations are conducted to test the effectiveness of the proposed bi-objective trajectory generation and the online modifications.

6.1. Optimization conditions

For the initial path generation, we choose the start point at $x = 1.0$ m, $y = -1.2$ m, and $z = 0.6$ m and the target point at $x = 1.0$ m, $y = 0.0$ m, and $z = 1.4$ m. The basement of the crane structure is located at $x = 0.0$ m, $y = 0.0$ m, $z = 0.0$ m with its center of rotation of the boom at $x = 0.0$ m, $y = 0.0$ m, $z = 1.3$ m. In order to create a safety margin, the tolerance values $[0.1, 0.1, 0.2]^T$ m are added to the original dimension of an obstacle $[0.7, 0.7, 1.1]^T$ for its length, width, and height, respectively. The corner point of the obstacle is located at $x = 0.6$ m, $y = -0.4$ m, $z = 0.0$ m, which are demonstrated in Fig. 3.

Considering the above simulation conditions, the A* algorithm generates the shortest-distance path in term of via-points in the Cartesian coordinate frame, which is transformed into the joint space using the inverse kinematics in Eq. (3). The crane parameters, used for generating optimal motion including the kinematics and dynamic constraints, are given in Table 1. These parameters are

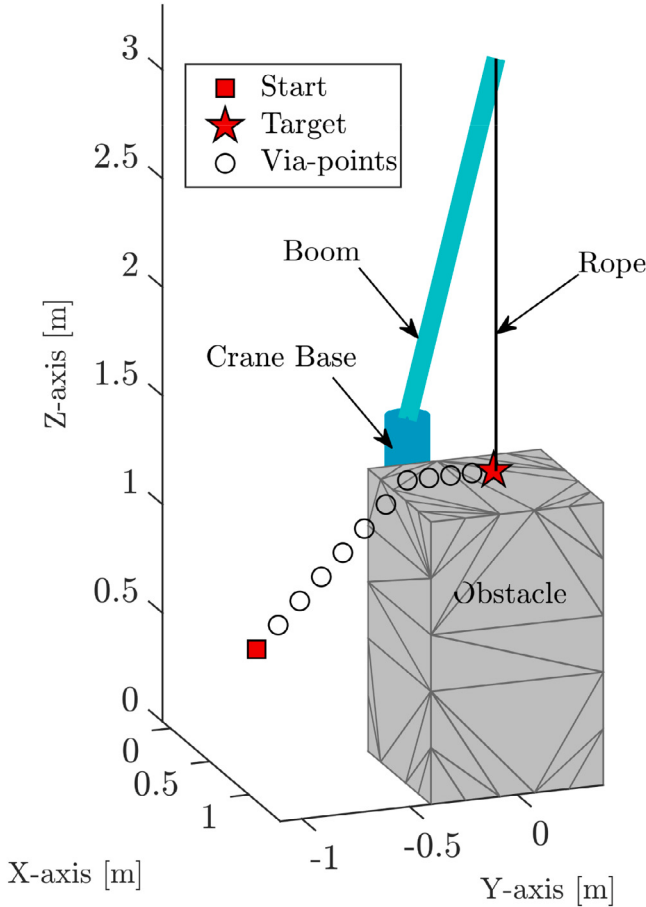


Fig. 3. Demonstration of the crane and obstacle location, and generation of collision-free via points by A* algorithm.

Table 1
Parameter values of the rotary crane system.

Parameter	Values	Parameter	Values
$\theta_{3,\max/\min}$ [deg/s]	± 4.35	$\theta'_{1,\max/\min}$ [deg/s]	± 0.5
$\theta_{5,\max/\min}$ [deg/s]	± 33.9	$\theta'_{2,\max/\min}$ [deg]	± 0.33
$\dot{l}_{\max/\min}$ [m/s]	± 0.43	$\theta'_{2,\max/\min}$ [deg/s]	± 0.5
$\theta_{1,\max/\min}$ [deg]	± 5	L [m]	2
$\theta_{1,\max/\min}$ [deg/s]	± 3	g [m/s ²]	9.81
$\theta_{2,\max/\min}$ [deg]	± 5	k [N m/deg]	2.42
$\theta_{2,\max/\min}$ [deg/s]	± 3	c [Pa.s/deg]	0.26
$\theta'_{1,\max/\min}$ [deg]	± 0.33	I [kg m ²]	54.95

determined based on the specifications of a real 3D rotary crane used in this study illustrated in Fig. 15(a), which is a 1 : 20 scaled model of an actual commercial crane. More details about the experimental setup are provided in Section 7. In this work, discrete grids $N = 12$ and $n = 36$ are used. The SQP (“fmincon” function in MATLAB) is employed to solve the OCP with a laptop computer with Windows 11 64-bit Intel(R) Core(TM) i7 – 1165G7 CPU @2.80 GHz and memory of 18 GB. The fmincon function is based on the sequential quadratic programming, which seems the most typical and reliable approach enabling to consider the complex nonlinear constraints, including the crane kinematics and dynamics, load sway, tower torsion, and obstacle avoidance. Additionally, general solvability of the proposed approach can be confirmed by using this typical solver. The nonlinear solver “fmincon” needs a feasible initial guess of the solution to guarantee convergence to an optimal solution that means the initial solutions has to fulfill the constraints of an OCP. Here, the initial B-spline control points are approximated only by fitting the least square function for the obstacle avoidance. With an appropriate guess of total motion time (i.e., $t_f > 0$), the initial trajectory satisfies the constraints. In order to compute the sway angles and velocities for the discrete time constraints, we use the “ode” function in MATLAB for solving the nonlinear dynamics in Eq. (1), where the initial sway angles and velocities are assumed zero, where no tower-torsion is assumed only at the start of the motion.

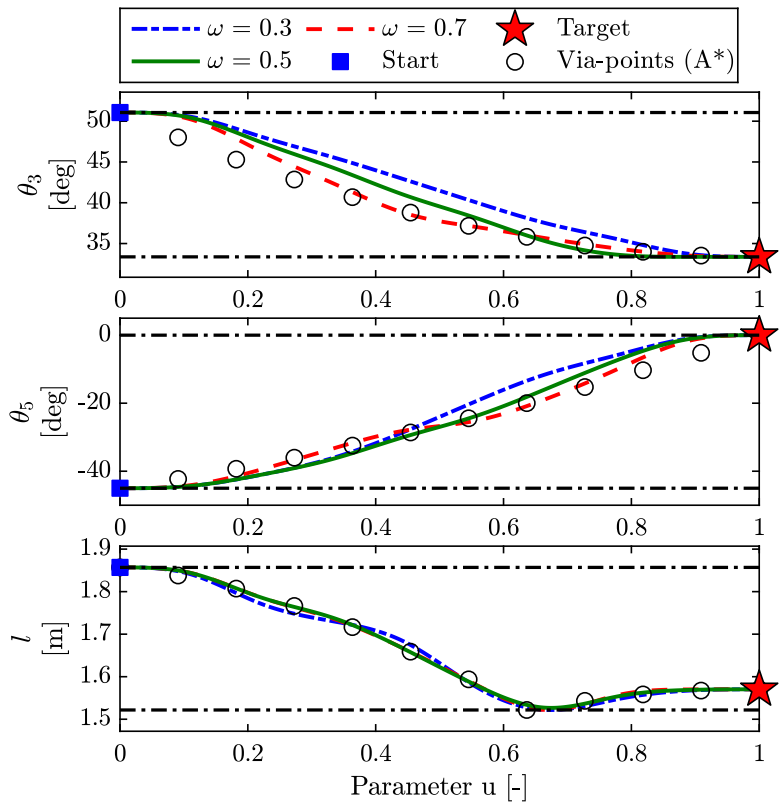


Fig. 4. Optimized actuator positions of vertical, horizontal, and rope length according to different weighting factors.

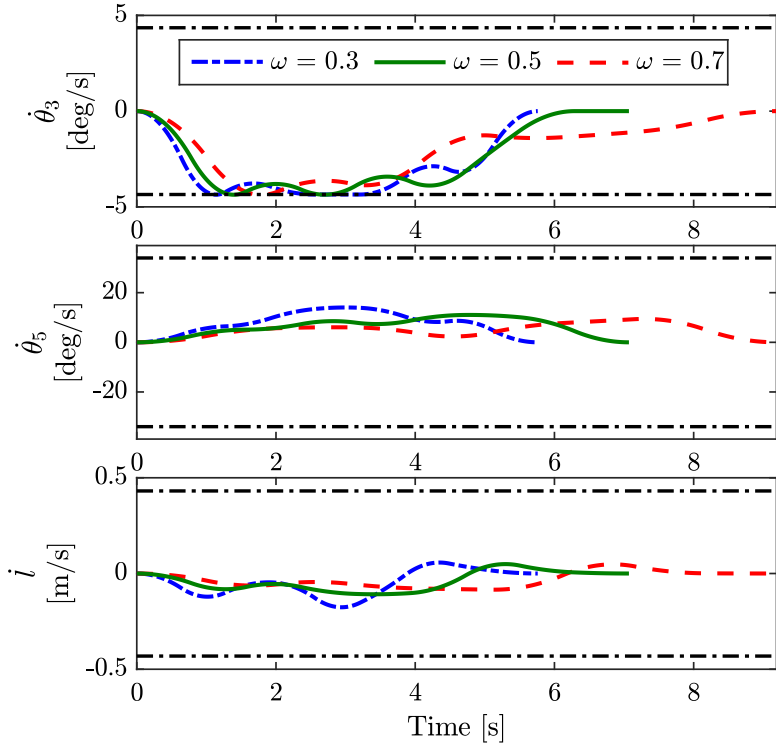


Fig. 5. Optimized actuator velocities of vertical, horizontal, and rope length according to different weighting factors.

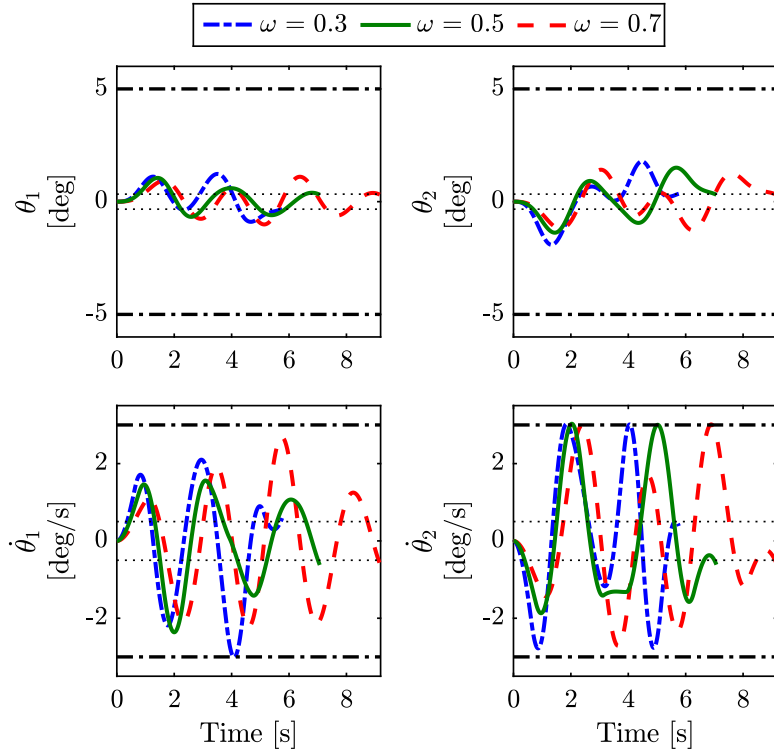


Fig. 6. Optimized sway positions and velocities according to different weighting factors.

6.2. Optimization results

This study firstly considers to optimize each of the objective functions in Eq. (9): the total motion time and the least square fitting function for the obstacle avoidance. The simulation results show that the motion time objective $f_{1,\min}$ satisfies all constraints at the time of $t_f = 6.3037$ [s] whereas its contradictory objective $f_{2,\min}$ gives the minimum solution at $t_f = 14.1865$ [s]. Thereafter, the normalization of each objective is implemented and the NNC method is used to generate the bi-objective solution with a specific trade-off corresponding the respective weighting factors.

In order to show the effectiveness of the weighting factor by our proposed method, we choose several values of weighing factors ω in Eq. (28) as 0.3, 0.5, and 0.7, respectively for trajectory optimization. Fig. 4 shows the horizontal and vertical boom angles, and the rope length according the different weighting factors. The respective actuator velocities are depicted in Fig. 5. Optimal sway positions and velocities, which satisfy the constraints are depicted in Fig. 6. The black central lines represent the upper and lower boundaries of the trajectories, and the black dot lines show the final upper and lower boundaries of the load-sway. For clear demonstration, the positions of the optimized trajectories with different weighting factors are compared in the parameter space (i.e., $u \in [0, 1]$) and its velocity, and the resulting load-sway conditions are compared in the time space (i.e., $t \in [0, t_f]$).

The weighting factor ω in Eq. (28) can be adjusted based on the requirements of specific application and environmental conditions. In some scenarios, where obstacles are in a safe condition, a weighting factor can be assigned to prioritize minimizing motion time. For example, the trajectory with the weighing factor $\omega = 0.3$ gives the time-optimality of 70% and the obstacle avoidance of 30% as presenting with the blue-dash line in Fig. 4; therefore, the generated positions are far from the A* via-points. Due to the time-optimality nature, the velocities hits the boundaries along the path, especially for the vertical boom; thus, the total motion time is minimized.

In contrast, the trajectory generated with a weighing factor $\omega = 0.7$ representing the time-optimality of 30% and the obstacle avoidance of 70% makes the control points of B-spline closer to the A* via points. As a result, the trajectories are closer to the via-points; therefore, obstacle avoidance is more guaranteed. To consider the equality ratio of trade-off for both objectives, the trajectory with a weighing factor of $\omega = 0.5$ is represented with the green lines in Fig. 4; thus the trajectory partly follows the obstacle avoidance scheme which hits the constraints for minimizing the motion time with an adequate load sway results. Regarding the effectiveness of the weighting factor ω on motion time values, Table 2 compares motion time required to generate the proposed trajectories for different weighting factor, where the equality ratio of the trade-off case requires intermediate motion time for transporting the load to its destination compared to other two cases. In order to realize the importance of weighting factor in trajectory optimization for satisfying obstacle avoidance, simulations of optimized 3D motions are depicted in Fig. 7. It is observed that 3D motions with high

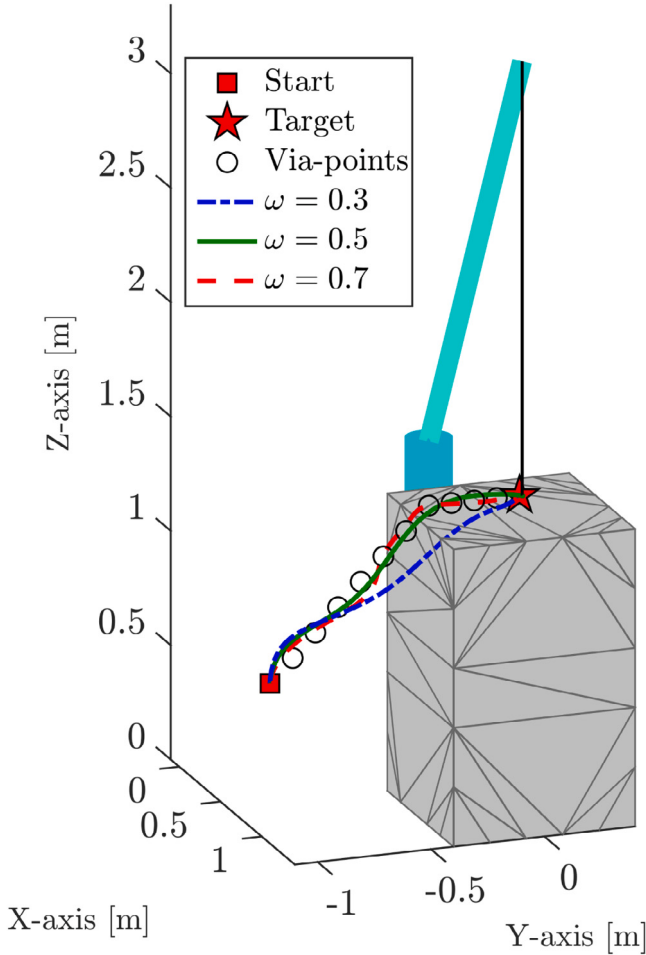


Fig. 7. Demonstration of optimized motions in 3D space according to different weighting factors.

Table 2

Motion time obtained by the proposed optimization for different weighting factor ω .

ω	Motion time in [s]
0.3	5.76
0.5	7.07
0.7	9.19

weighting factors (i.e., $\omega = 0.5$ and $\omega = 0.7$) guaranteed obstacle avoidance scheme provided by A* algorithm. On the other hand, the motion with a low weighting factor $\omega = 0.3$ does not satisfy obstacle avoidance scheme. Therefore, it is important to notice that low weighting factors must not be used for the real crane system. Since several constraints are required to consider to formulate the OCP, the computation time for running the problem takes 286.41[s] on an average, which may be challenging to implement on online applications.

6.3. Polynomial-based optimal trajectory

To evaluate the effectiveness of the proposed optimization approach, the trajectory generated with a weighting factor of $\omega = 0.3$ is compared with a previous work using the same constraints and the two contradictory objectives: the total motion time and the least square fitting function [23]. In the previous approach, the sixth-order polynomial trajectories have been generated for the horizontal and vertical boom angles, and the rope motion, as follows:

$$\begin{aligned} \theta_3 &= c_{v6} T_1^6 + c_{v5} T_1^5 + c_{v4} T_1^4 + c_{v3} T_1^3 + c_{v2} T_1^2 + \theta_3^{int} \\ \theta_5 &= c_{h6} T_1^6 + c_{h5} T_1^5 + c_{h4} T_1^4 + c_{h3} T_1^3 + c_{h2} T_1^2 + \theta_4^{int} \\ l &= c_{r6} T_1^6 + c_{r5} T_1^5 + c_{r4} T_1^4 + c_{r3} T_1^3 + c_{r2} T_1^2 + l^{int} \end{aligned} \quad (37)$$

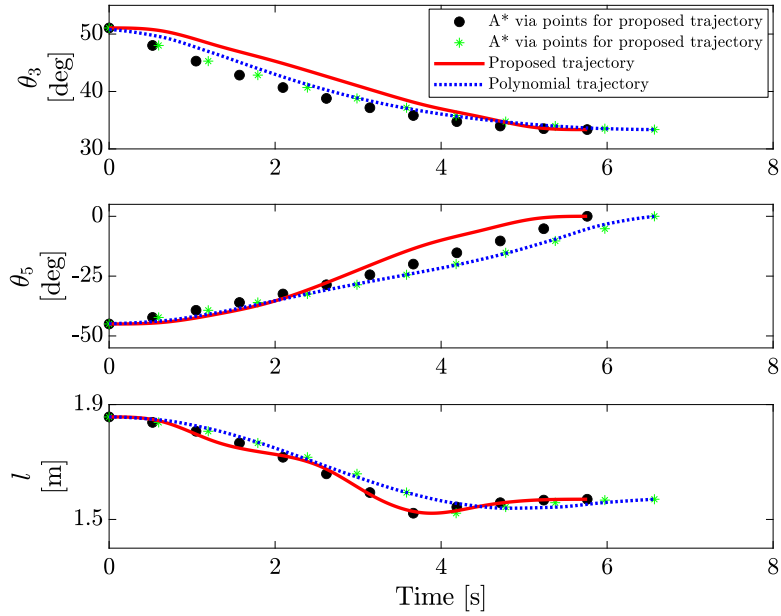


Fig. 8. Proposed trajectories for the vertical and horizontal boom angles, and the rope length generated with a weighing factor of $\omega = 0.3$ compared with trajectories in Eq. (37).

where the optimal polynomial coefficients c_{vu} , c_{hu} , and c_{ru} , where $(u = 2, \dots, 6)$ are determined through the optimization. The initial positions in the joint space are represented as θ_3^{int} , θ_5^{int} , and l^{int} for the vertical and horizontal boom angles, and the rope length, respectively. The motion time $T_1 = dT$, where d is a vector containing discrete values from 0 to 1 ($0 \leq d \leq 1$), and T represents the total motion time required for deriving the crane load into destination.

The contradictory objectives of generating a polynomial sixth-order trajectory are formulated as follows:

$$f_p = w_t T + w_3 \sum_{i=1}^N (\theta_{3i}^* - \theta_{3i})^2 + w_5 \sum_{i=1}^N (\theta_{5i}^* - \theta_{5i})^2 + w_r \sum_{i=1}^N (l_i^* - l_i)^2 \quad (38)$$

where w_t represents the time weight, and N denotes the number of collision-free via-points generated by the A* algorithm explained in Section 2.2. The vertical and horizontal boom angles obtained from the A* algorithm are represented by θ_{3i}^* and θ_{5i}^* , respectively, with their corresponding weight values represented by w_3 and w_5 . Similarly, l_i^* represents the rope length derived from the A* algorithm, and its associated weight is w_r . The time weight w_t is assigned a value of 1, while the other weights are normalized based on the following criteria:

$$\begin{aligned} w_3 &= 1/(\theta_{3\max}^* - \theta_{3\min}^*)^2 \\ w_5 &= 1/(\theta_{5\max}^* - \theta_{5\min}^*)^2 \\ w_r &= 1/(l_{\max}^* - l_{\min}^*)^2 \end{aligned} \quad (39)$$

where l_{\max}^* and l_{\min}^* represent the maximum and minimum values of the A* rope length, respectively. $\theta_{3,\max}^*$, $\theta_{3,\min}^*$, $\theta_{5,\max}^*$, and $\theta_{5,\min}^*$ correspond to the maximum and minimum values for the vertical and horizontal boom rotations generated by the A* algorithm. The optimization problem for generating a polynomial sixth-order trajectory is formulated as follows:

$$\min_{T, v_u, h_u, r_u} f_p \quad (40)$$

To ensure a fair comparison with the proposed approach, the same constraints of the crane kinematics, load sway, and tower torsion effect have been applied. Fig. 8 compares the proposed trajectories for the vertical and horizontal boom angles, and the rope length with the sixth-order polynomial trajectories. Both approaches effectively follow the collision-free via-points obtained by the A* algorithm, ensuring obstacle avoidance. The computational and motion time required to generate the proposed trajectories are 665.48 and 5.67, respectively. In contrast, the polynomial trajectories require 114.71 s for computation and 6.57 s for motion time. In each case, at least one of the trajectories (e.g., the vertical boom motion) reaches the velocity limits, guaranteeing time-optimality of the trajectory. According to swaying angles suppression, load sway profiles produced by both schemes are compared in Fig. 9, where load sway constraints have been satisfied. Although, the proposed approach achieves a shorter motion time compared to the polynomial-based optimal trajectory in Eq. (37), it results in nearly the same load sway magnitudes for the radial and tangential directions to the horizontal boom motion, respectively.

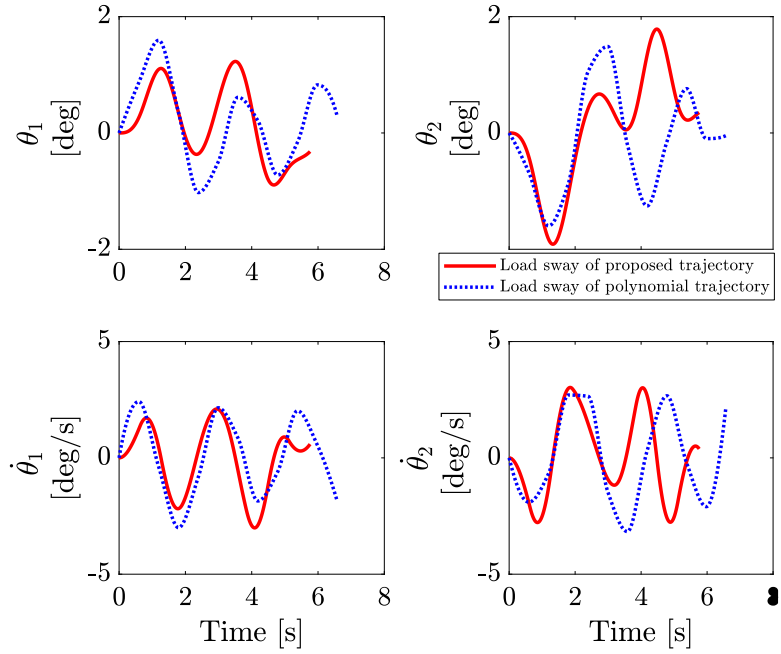


Fig. 9. Load sway profiles generated by proposed trajectories with a weighing factor of $\omega = 0.3$ compared with the ones generated by trajectories in Eq. (37).

6.4. Modification conditions

In this section, we implemented simulations on modification of an optimal trajectory for online applications. Different DOFs (i.e., horizontal angle θ_5 or vertical angle θ_3 or rope length l) are chosen in order to test the performance of the proposed modification method, and the optimal trajectories are compared in terms of total motion time, obstacle avoidance scheme, and the computation time. Firstly, the modified target positions are transformed into the respective joint coordinates and the SFs are determined. The OCPs are solved with a laptop computer with the same specifications under the same set of discrete constraints in optimization. The original trajectory with a weighting factor of $\omega = 0.5$ is chosen for modification due to the advantage of contributing the equal trade-off between the total motion time, obstacle avoidance scheme, and the load-sway results. For modification, we choose two targets: MT1 and MT2, which are relocated $+0.25$ [m] and -0.25 [m] distance apart from the original target, respectively as shown in Fig. 10. The system parameters and constraints are the same as previous optimization. In addition, we set the constraint for avoiding the obstacle c_{diff} as 4.68 [deg], 11.27 [deg], and 0.32 [m] for each DOF motion: the horizontal and vertical boom angles, and the rope length, respectively. For the initial guess for solving 1-DOF modifications, we use the optimized solutions in Section 6.2 due to the similarity of the trajectories.

6.5. Modification results

Position profiles for the modified target MT1 and MT2 are depicted in Figs. 11(a) and 11(b), which compares different online modifications: the SF, the horizontal and vertical boom modifications: θ_5 and θ_3 , and the rope length modification l with the optimized trajectory. It is observed that the SF satisfies the final target positions by scaling each optimized trajectory's position. For 1-DOF modifications, the modified positions reach the respective targets for MT1 and MT2 by allowing changes in each DOF motion. The modified trajectories are resembled and near to the optimized trajectory due to the added constraint in Eq. (36). The velocity profiles of the respective 1-DOF modifications for the modified target MT1 and MT2 are compared in Figs. 12(a) and 12(b), respectively. In Fig. 12(a), the SF violates velocity constraints especially for the vertical boom motion (see enlarged view). The reason is that the optimized trajectory already hits the maximum/minimum velocity constraint, and the SF amplifies optimized trajectories within the same total motion time. In other words, the optimization variables (i.e., the total motion time and the B-spline control points) must modify simultaneously to meet the required constraints. In 1-DOF modification, we modify the total motion time and 1-DOF B-spline control points by optimization; therefore, all the modified trajectories satisfy the constraints. Moreover, the initial and target velocities and accelerations are zeros, which lead to the smooth starting and ending transitions. Due to the longer distance target MT1 ($+0.25$ [m]), the θ_3 , θ_5 , and l modifications spend the respective total motion times of 12.44% , 7.63% , and 5.65% more than the SF trajectory. As a benefit, all constraints along the horizon are guaranteed in our proposed method. The velocity profiles in Fig. 12(b) show that the SF method does not violate the constraints under the same total motion time as the original trajectory; however in this case, the time-optimality is not achieved (i.e., at least one of the trajectories does not reach the max/min limit).

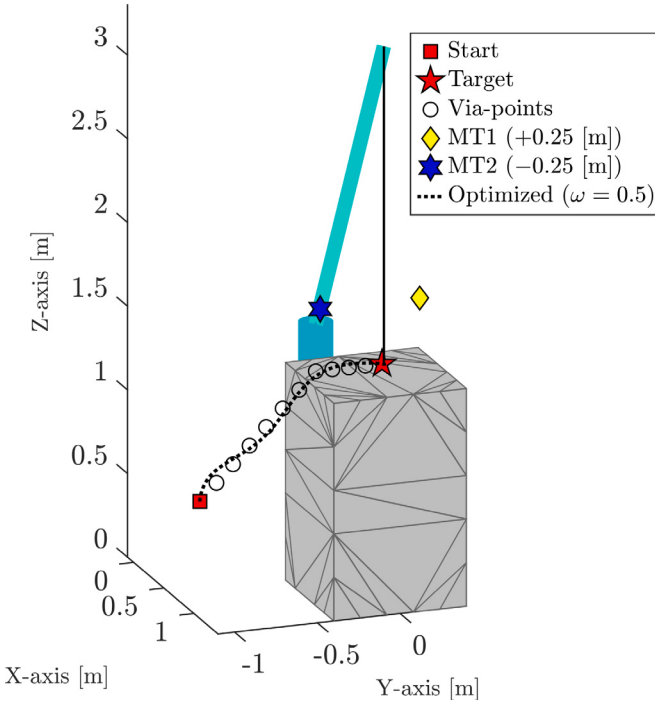


Fig. 10. Demonstration of modified targets MT1 and MT2 compared to the original target in 3D space.

However, 1-DOF modification provides both the optimal motion and the constraint satisfaction. Due to the shorter distance target MT2 (-0.25 [m]), the θ_3 , θ_5 , and l modifications save total motion time about 3.39%, 5.54%, and 4.84% than the SF method.

Comparing the load-sway result, the SF method violates the constraints whereas the 1-DOF modifications satisfy for all including the final sway conditions (see Fig. 13(a) for MT1 and Fig. 13(b) for MT2). Additionally, Table 3 summarizes the average values of absolute load swaying angles for the two modified positioning targets MT1 and MT2. The table presents load sway produced by the optimal trajectory and the scaling factor method compared with these values produced by the different modification modes, including the vertical angle θ_3 , horizontal angle θ_5 , and rope length l . The proposed trajectory by the rope length l modification resulted in smaller load sway compared to other methods, including the original trajectory. Moreover, the trajectories modified by the proposed method hit the maximum/minimum limits of the constraints, which guarantee time-optimality of the trajectory, especially the sway velocities for θ_2 . Additionally, the constraint on B-spline control points in Eq. (36) makes the modified trajectories closer to the optimized one; therefore, the generated paths satisfy the obstacle avoidance scheme as well as satisfying all constraints, which are depicted in Figs. 14(a) and 14(b) for MT1 and MT2, respectively.

An important factor to consider is the computation time of the modified trajectories. Comparison of the total motion time and computation time for different modification modes are given in Table 4. The computation times are counted for 5 trials and the average computation time for each motion is determined. The SF method multiplies the original trajectories which does not reformulate the optimal control problem; thus the computation time is very small approximately 0.01 [s]. In the proposed 1-DOF modification method, the number of optimization variables are reduced in the optimal control problem to save the computational efficiency. As a result, the average computation time required for θ_3 , θ_5 , and l modifications are 3.48 [s], 2.60 [s], and 3.66 [s], respectively, which are 82-times, 110-times, and 78-times faster than that of the original optimized trajectory; therefore, it is practical to use for the online applications.

7. Experiment

7.1. Experimental conditions

In order to show the effectiveness of our proposed method, the simulation results are verified with a lab-scale 3D rotary crane with a tower-torsion effect, which is the 1 : 20 scale of the actual crane. The experimental setup is illustrated in Fig. 15(a), while the spring-damper mechanism used to simulate the horizontal tower-torsion effect is depicted in Fig. 15(b). The system includes three AC motors for driving the vertical and horizontal boom angles θ_3 and θ_5 , and the rope length l . The movement of crane and load sway is detected with the motion capture system, where eight cameras are used to measure the sway angles θ_1 and θ_2 , the vertical and horizontal (before and after a tower-torsion generator) boom angles θ_3 , θ_5 , θ_4 , and the rope length l motion in real-time. The corresponding velocities are estimated by the numerical differentiation of position measurements. The resolution of

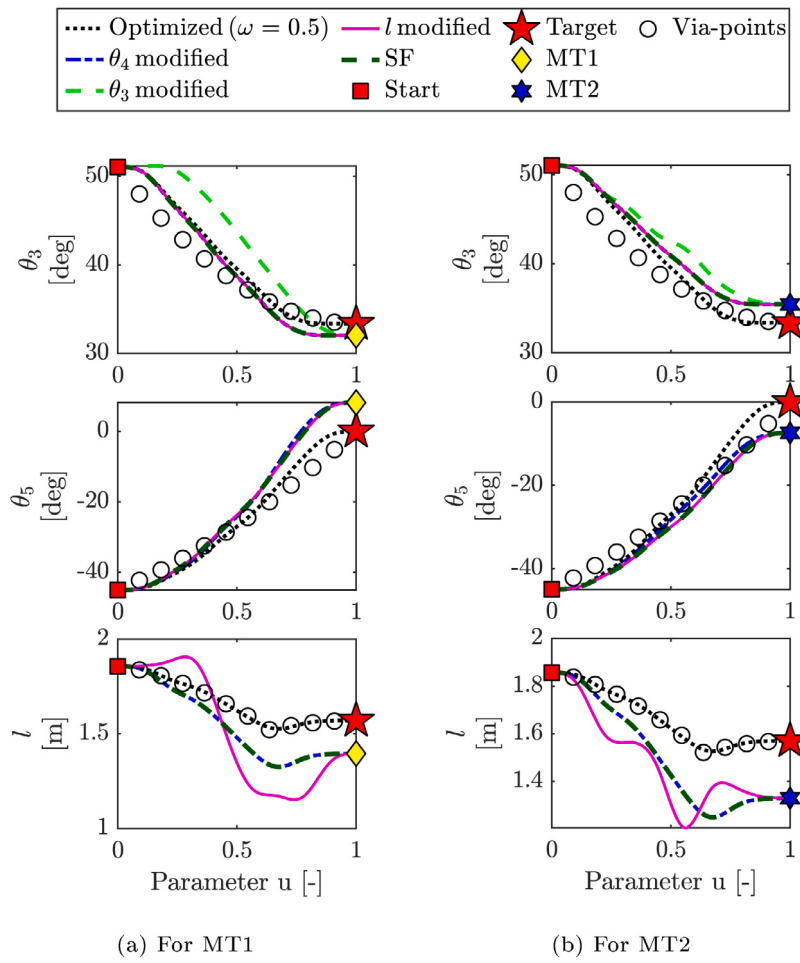


Fig. 11. Comparison of optimized and modified actuator positions according to the target MT1 and MT2.

Table 3

Average values of absolute load swaying angles for the original trajectory, the SF modified one, and the proposed method with two different target positions.

Methods	Load sway in deg			
	MT1		MT2	
	θ_1	θ_2	θ_1	θ_2
Original	0.41	0.68	0.41	0.68
SF	0.35	0.63	0.40	0.68
θ_3	0.29	0.67	0.42	0.73
θ_5	0.48	0.70	0.42	0.62
l	0.35	0.63	0.40	0.70

Table 4

Comparison of total motion time and average computation time of the SF and the proposed methods with different target positions.

Methods	Total motion time [s]		Average computation time [s]	
	MT1	MT2	MT1	MT2
SF	7.07	7.07	0.01	0.01
θ_3	7.95	6.83	5.59	1.38
θ_5	7.61	6.68	0.39	4.82
l	7.47	6.69	2.34	4.98

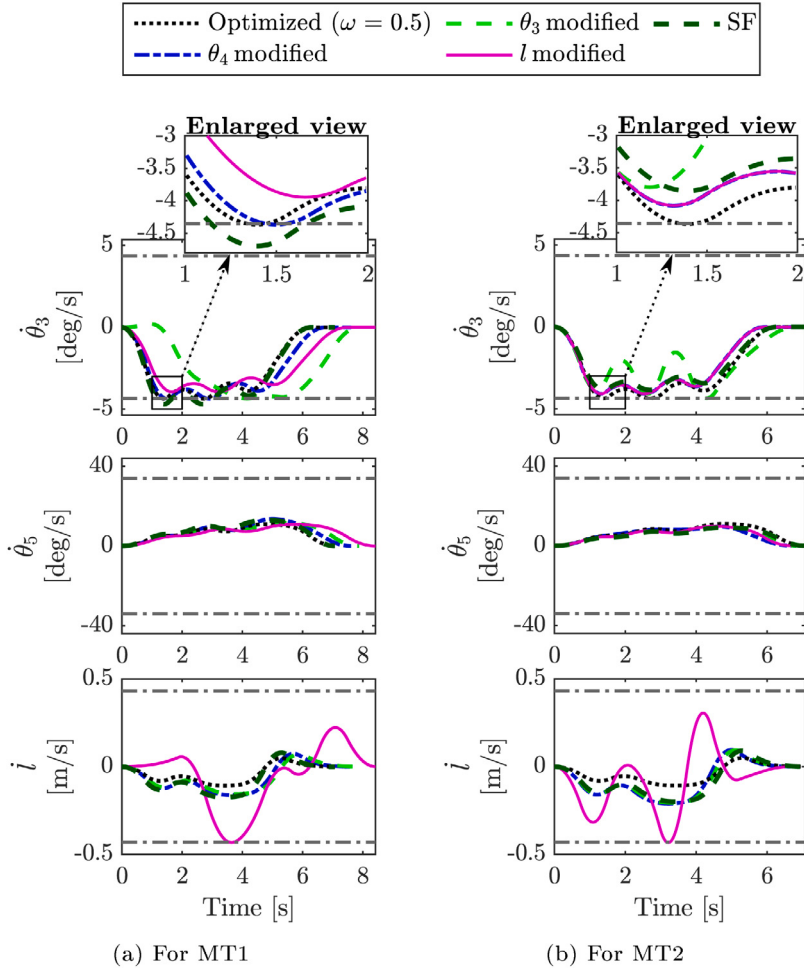


Fig. 12. Comparison of optimized and modified actuator velocities according to the target MT1 and MT2.

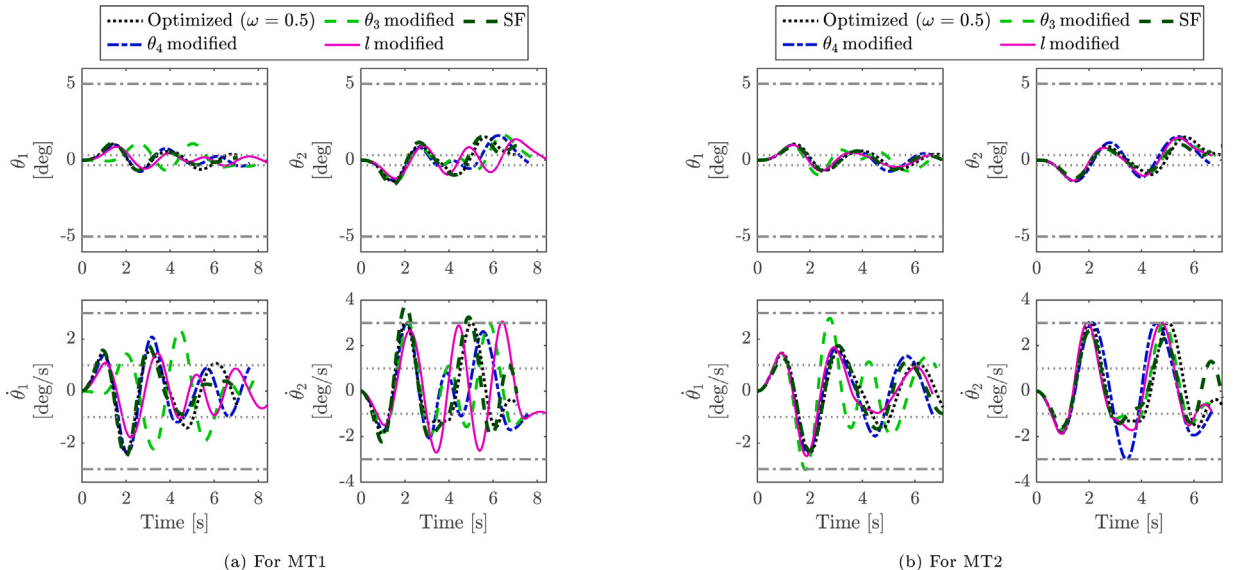


Fig. 13. Comparison of optimized and modified sway positions and velocities according to the target MT1 and MT2.

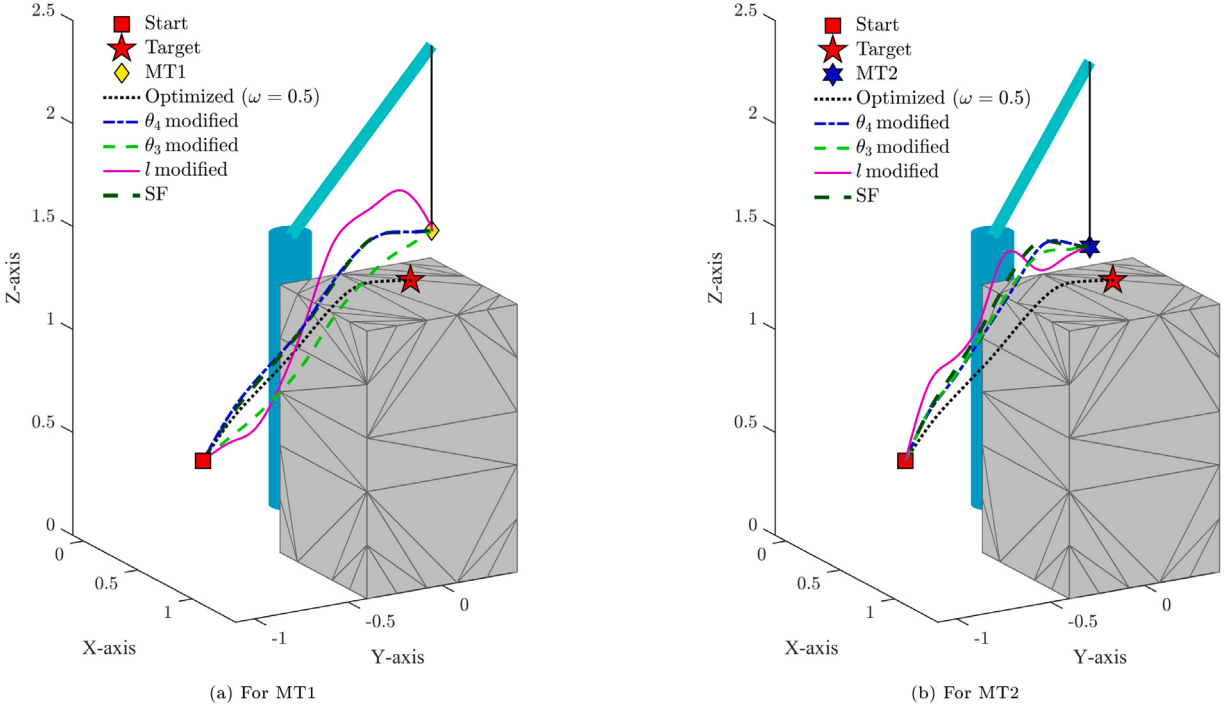


Fig. 14. Demonstration of modified motions for MT1 and MT2 in the three-dimensional space.

Table 5

Experimental comparison of maximum load swaying angles for the proposed optimization with different weighting factor ω .

ω	Load sway in deg	
	θ_1	θ_2
0.3	3.125	1.875
0.5	0.875	1.813
0.7	2.188	0.937

the camera is 1280×1024 pixel and the frame rate is 100 [fps]. Moreover, the load with a unit mass is hanged at the tip of the wire rope with a hook. The obstacle is represented by a carton box with a dimension of $0.8 \times 0.8 \times 1.3$ [m^3], and is placed at $x = 0.6$ [m], $y = -0.4$ [m], $z = 0.0$ [m]. The velocity trajectories are processed in Simulink model (MATLAB), which is linked with the sBOX digital signal processor to import the corresponding voltage signals to the crane with a sampling time of 10 [ms]. For verification, the experimental results are discussed in two subsections: bi-objective optimization results in Section 6.2 and trajectory modification results in Section 6.5.

7.2. Experimental validation for optimization results

We conduct the experiments of the optimized trajectory with the corresponding weighting factors: $\omega = 0.3$, $\omega = 0.5$, and $\omega = 0.7$ in Section 6.2 to validate the effectiveness of the proposed bi-objective optimization method. Fig. 16 shows the comparison of simulation and experimental positions according to the different weighting factors, and their corresponding velocities in Fig. 17. It is observed that experimental positions reach their respective targets with the absolute average accuracy of 0.89 [deg], 1.14 [deg], and 0.03 [m] for the vertical and horizontal boom angles, and for the rope length, respectively. It is also verified that trajectories with the high weighing factor $\omega = 0.7$ are near to the A* via-points, thus satisfy the obstacle avoidance scheme. As a contradictory, the total motion time is slower. Trajectories with moderate weighting factor $\omega = 0.5$ plays the equal trade-off between the total motion time and obstacle avoidance scheme, and the trajectories with the least weighting factor $\omega = 0.3$ gives the fastest total motion time. The generated sway positions and velocities validate with the simulation results along the horizon as shown in Fig. 18. Additionally, Table 5 compares the maximum experimental values of load swaying angles for different weighting factors, where the proposed trajectory generated with the equality trade-off ratio provides load sway less than 2 degrees for both directions. Therefore, the above-mentioned results prove that the proposed method is effective for bi-objective trajectory generation for a specific trade-off between contradictory objectives for rotary crane systems.

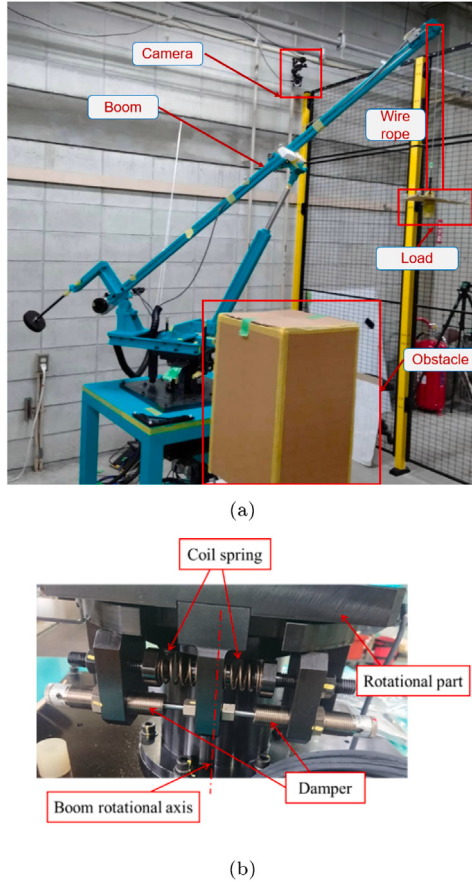


Fig. 15. Experimental setup of a lab-scale 3D crane system.

Table 6

Experimental comparison of maximum load sway angles to modified target position MT1 for the original trajectory, the SF modified one, and the proposed method.

Modification	Load sway in deg	
	θ_1	θ_2
Original	0.875	1.875
SF	0.937	0.813
θ_3	1.88	1.25
θ_5	1.813	1.88
l	1.25	1.87

7.3. Experimental validation for modification results

We conduct the experiments for the modified target MT1 according different modes of 1-DOF modification(i.e., θ_3 , θ_5 , and l) and the SF. Fig. 19 presents the experimental vertical and horizontal boom angles, and the rope length for the modified target MT1 compared to the original optimized trajectory. The results shows that the SF and all 1-DOF modified trajectories reach their respective targets for MT1 with absolute average errors of 1.06 [deg], 0.41 [deg], and 0.04 [m] for θ_3 , θ_5 , and l , respectively. Therefore, the crane successfully carries the load from the start to the modified target MT1. The comparison of simulation and experiment velocities are depicted in Fig. 20. It is observed that all reference velocities are well-tracked by the crane system, which validates the simulation results. Another important thing to verify is the satisfaction of load-sway angles along the modified paths. Fig. 21 shows that the generated sway results from our proposed method keeps a similar vibration property as the optimized trajectory. In addition, Table 6 summarizes the maximum amplitudes of load sway angles for modified positioning target MT1, where the optimal trajectory and the scaling factor method are compared considering the different modification modes. The modified trajectory based on the rope length l agrees with the simulation results, in that it provides smaller load sway compared to other methods. Above-mentioned results clearly states that experiments are well-aligned with simulations and the proposed trajectory generation and modification

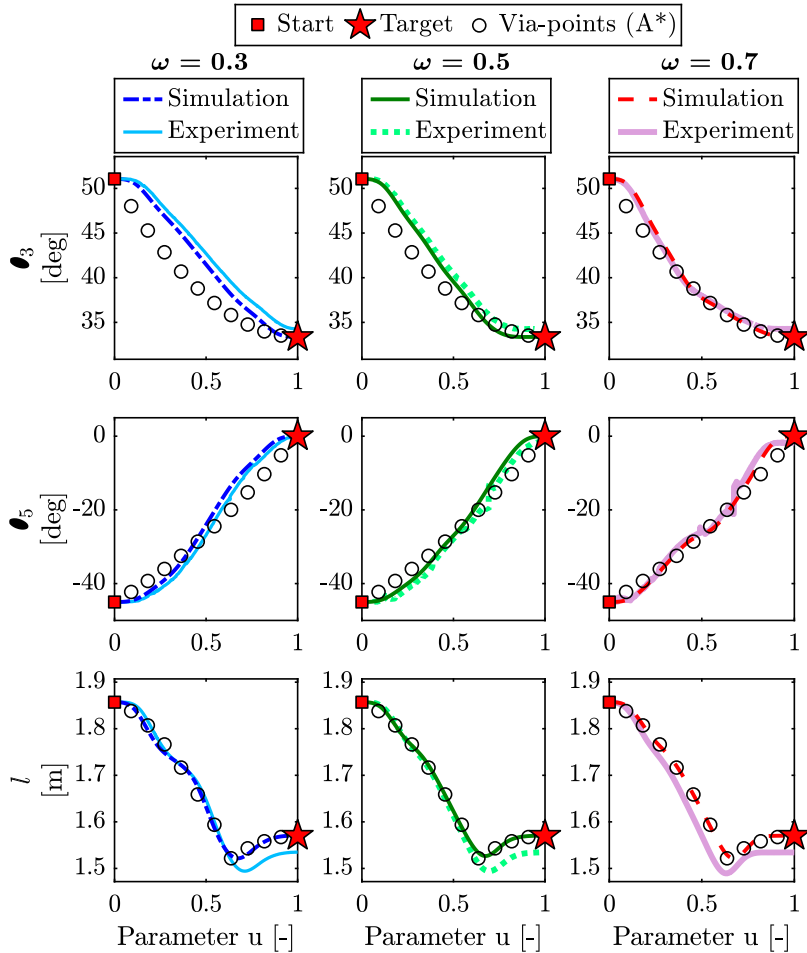


Fig. 16. Experimental results of the optimized actuator positions according to different weighting factors.

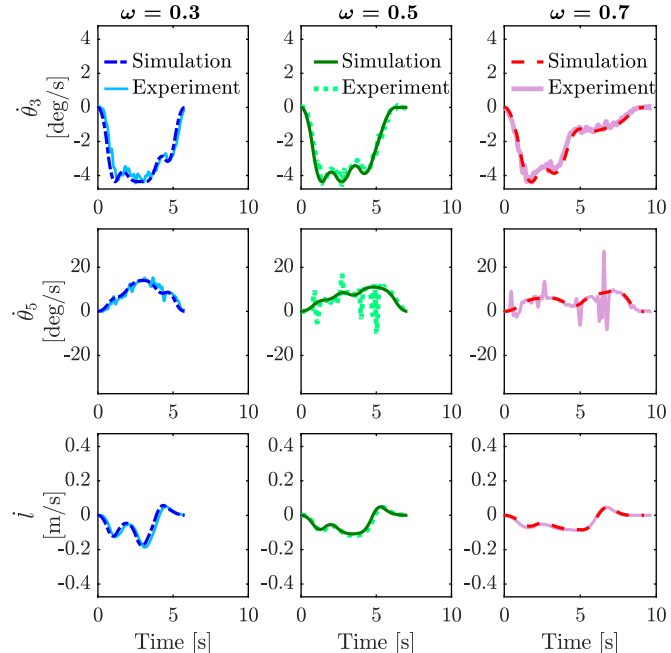


Fig. 17. Experimental results of the optimized actuator velocities according to different weighing factors.

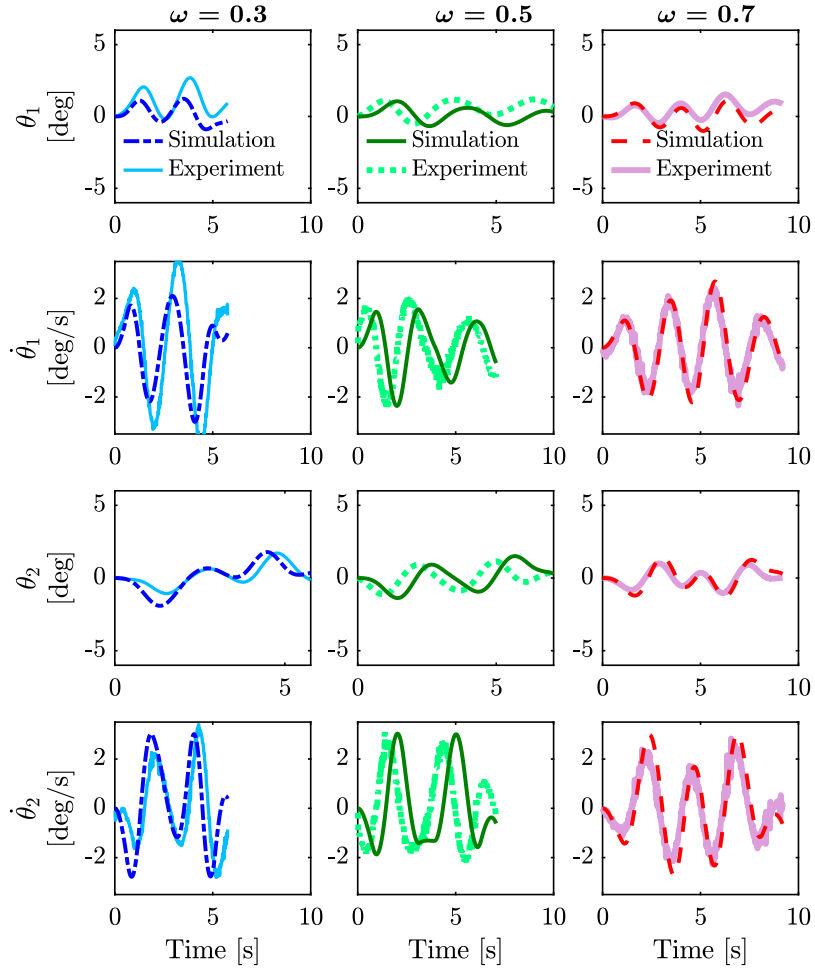


Fig. 18. Experimental results of load-sway positions and velocities according to different weighting factors.

methods are effective for improving the performance of machines (e.g., productivity and obstacle avoidance) without an additional hardware setup and for the practical usage for trajectory modifications in online applications.

8. Conclusions and future works

In this paper, we present an algorithm for accurately positioning the load-sway in an optimal motion time considering obstacle avoidance, kinematic, and dynamic limitations of the system, as well as modifying the trajectory online without violating system constraints in a short amount of computation time. The first section of the paper describes the offline bi-objective OCP formulation between the contradictory objectives of total motion time and the least square fitting for obstacle avoidance. The weight may be defined by the user and a specific trade-off nature is explored by applying the NNC and the direct transcription methods. We parameterize the trajectory in terms of cubic B-splines; therefore, the velocity and acceleration continuities of the trajectory are guaranteed. The optimized offline trajectory satisfies all the constraints along the horizon, although the computation time is large. Therefore, when the target/start position of the load changes, it is challenging to be able to use online.

The second section presents the trajectory modification method without computing the entire OCP. This method uses only 1-DOF motion of the crane and the total time to update the original trajectory, thus it reduces the optimization variables from computing the OCP. As a result, an optimal trajectory that satisfies all constraints can be generated within the practical computation time. An additional constraint is proposed in such a way that the modified trajectory has a certain freedom to move near the original one; therefore, obstacle avoidance scheme is satisfied. Since the above limitation depends on the trade-off level of the bi-objective problem, the authors recommend to choose base optimal trajectories with a good trade-off for guaranteeing obstacle avoidance. The simulation and experimental results proved that the proposed method provides the optimal trajectory generation of flexible rotary cranes for load-sway reduction that includes an obstacle avoidance scheme in a practical computation time.

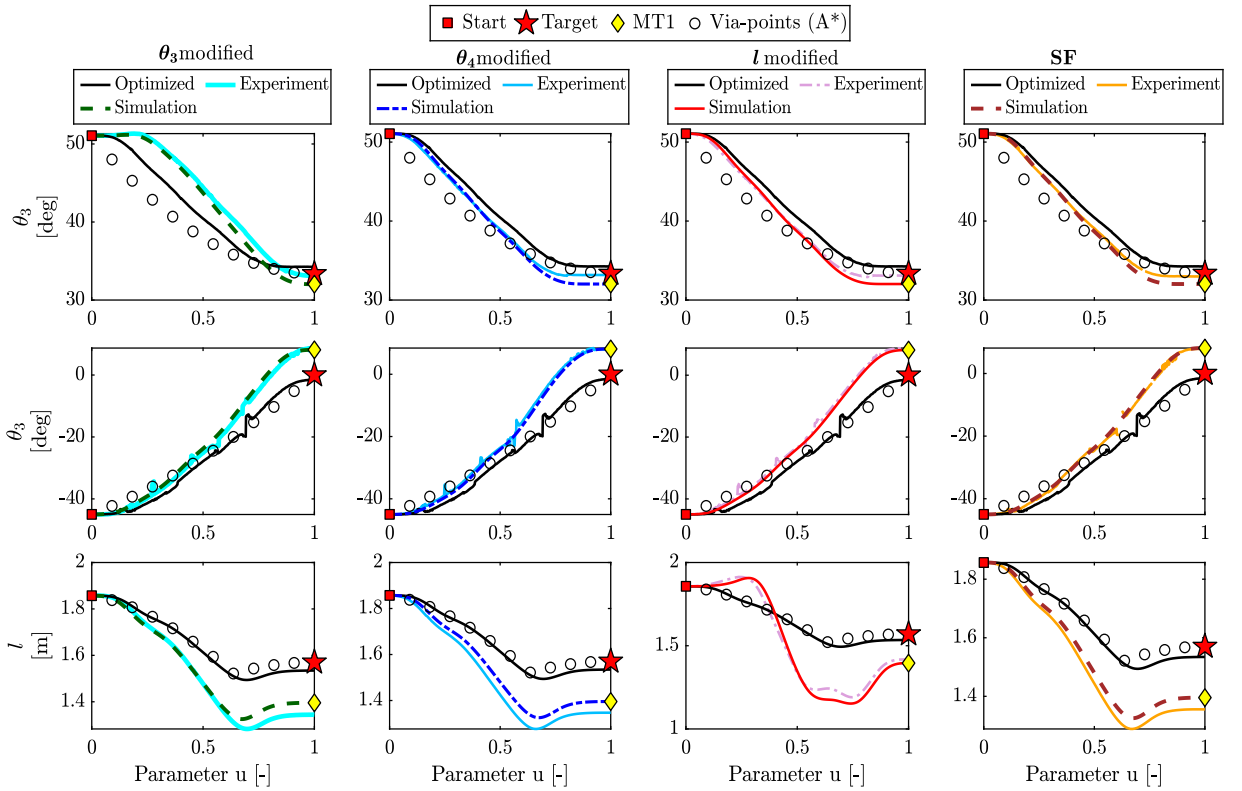


Fig. 19. Experimental actuator positions for modified target MT1 with different modes of modification methods.

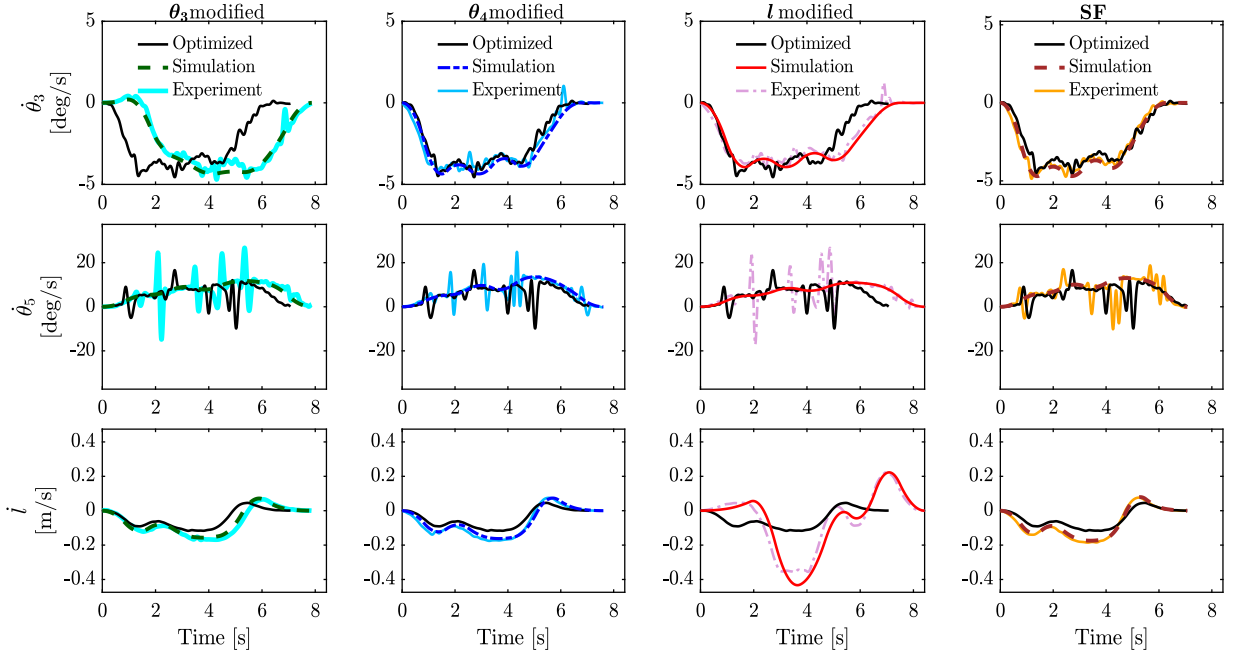


Fig. 20. Experimental actuator velocities for modified target MT1 with different modes of modification methods.

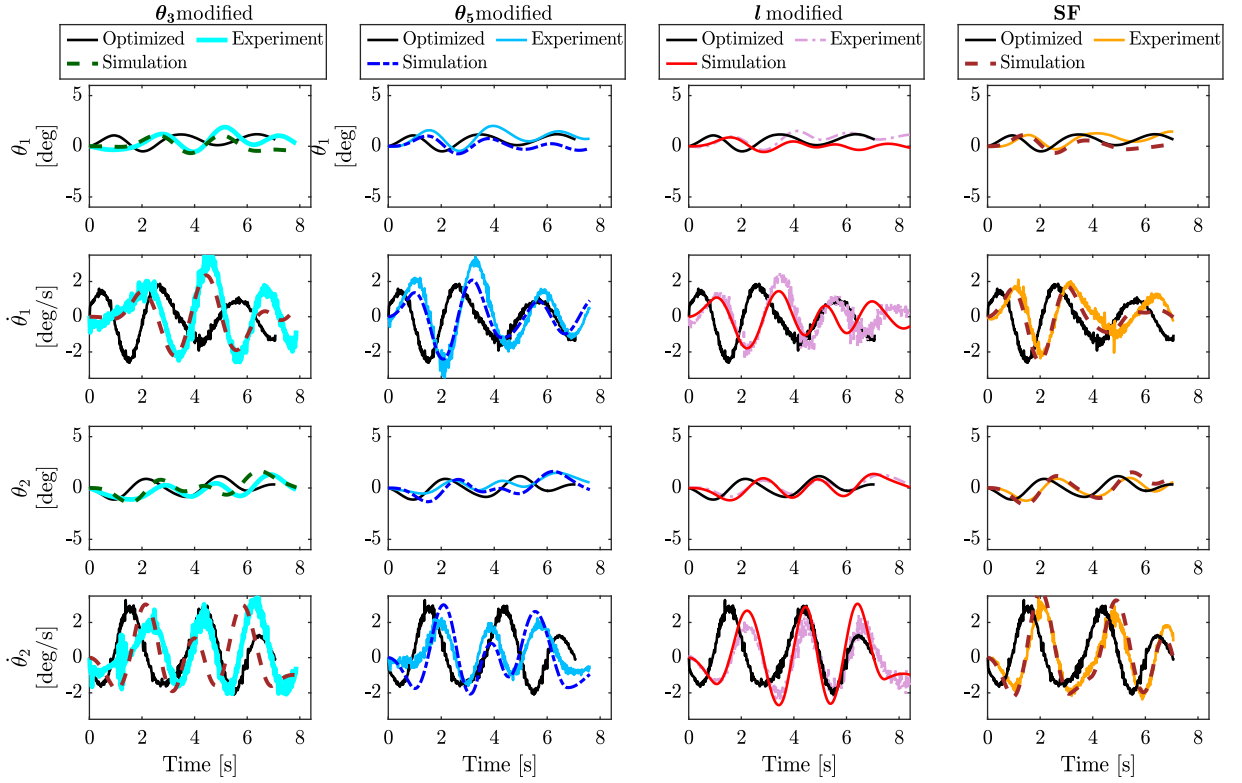


Fig. 21. Experimental load-sway results for modified target MT1 with different modes of modification methods.

CRediT authorship contribution statement

Abdallah Farrage: Writing – review & editing, Validation, Investigation. **Min Set Paing:** Writing – review & editing, Writing – original draft, Visualization, Validation, Methodology. **Nur Azizah Amir:** Writing – review & editing. **Hideki Takahashi:** Project administration, Investigation. **Shintaro Sasai:** Project administration, Investigation. **Hitoshi Sakurai:** Project administration, Investigation. **Masaki Okubo:** Project administration, Methodology, Investigation. **Naoki Uchiyama:** Writing – review & editing, Validation, Project administration, Investigation.

Declaration of competing interest

The authors declare the following financial interests/personal relationships which may be considered as potential competing interests: Min Set Paing reports financial support was provided by Kobelco Construction Machinery Co Ltd. If there are other authors, they declare that they have no known competing financial interests or personal relationships that could have appeared to influence the work reported in this paper.

Appendix

The pseudo-codes for the main algorithms are provided to clarify the approach steps. First, the summarized code, which executes bi-objective optimal trajectory generation to minimize the motion time and reduce the risk of collision with obstacles, is presented as follows:

1. Generate collision-free via points of the motion trajectory using the A* algorithm assuming no load sway [37].
2. Represent the motion trajectory by B-splines in Eq. (11).
3. Find optimal parameter values ϕ in Eq. (17), i.e., B-spline coefficients and minimal motion time, by solving Eq. (23) to obtain \bar{F}_1 and \bar{F}_2 in Eqs. (24) and (25), which consider the load sway and tower torsion of the crane using the dynamics in Eq. (1).
4. Solve Eqs. (26)–(28) to obtain the bi-objective optimal trade-off solution of the motion trajectory based on the ω value.

Second, the pseudo-code, which clarifies the steps of the online modification approach, is summarized as follows:

1. Determine the new target load positions and their corresponding values into the joint space using the inverse kinematics scheme in Eq. (3).
2. Calculate the SF weights in Eq. (29) for initializing the trajectory and updating the initial control point of B-spline in Eq. (30).
3. Determine the corresponding position, velocity, and acceleration for the modified trajectory in Eqs. (11)–(14).
4. Consider only 1-DOF control variables and the motion time to modify the original optimal trajectory.
5. Find optimal parameter values ϕ in Eq. (35) to obtain t_f in the sub-OCP written in Eq. (34) with considering the additional constraint in Eq. (36) to guarantee collision avoidance.
6. Solve Eq. (34) to obtain the modified trajectory satisfying the constraints.

Data availability

Data will be made available on request.

References

- [1] J. Li, L. Bai, W. Gao, N. Shi, N. Wang, M. Ye, H. Gu, X. Xu, J. Liu, Reliability-based design optimization for the lattice boom of crawler crane, *Structures* 29 (2021) 1111–1118.
- [2] Y. Li, X. Xi, J. Xie, C. Liu, Study and implementation of a cooperative hoisting for two crawler cranes, *J. Intell. Robot. Syst.* 83 (2016) 165–178.
- [3] H. Takahashi, A. Farrage, K. Terauchi, S. Sasai, H. Sakurai, M. Okubo, N. Uchiyama, Sensor-less and time-optimal control for load-sway and boom-twist suppression using boom horizontal motion of large cranes, *Autom. Constr.* 134 (2022) 104086.
- [4] Y. Fang, Y.K. Cho, J. Chen, A framework for real-time pro-active safety assistance for mobile crane lifting operations, *Autom. Constr.* 72 (2016) 367–379.
- [5] L.A. Tuan, S.-G. Lee, D.H. Ko, L.C. Nho, Combined control with sliding mode and partial feedback linearization for 3D overhead cranes, *Internat. J. Robust Nonlinear Control* 24 (18) (2014) 3372–3386.
- [6] D. Liu, J. Yi, D. Zhao, W. Wang, Adaptive sliding mode fuzzy control for a two-dimensional overhead crane, *Mechatronics* 15 (5) (2005) 505–522.
- [7] J.H. Yang, K.S. Yang, Adaptive coupling control for overhead crane systems, *Mechatronics* 17 (2–3) (2007) 143–152.
- [8] H.M. Omar, A.H. Nayfeh, Gantry cranes gain scheduling feedback control with friction compensation, *J. Sound Vib.* 281 (1–2) (2005) 1–20.
- [9] K. Zavari, G. Pipeleers, J. Swevers, Gain-scheduled controller design: illustration on an overhead crane, *IEEE Trans. Ind. Electron.* 61 (7) (2013) 3713–3718.
- [10] T. Yang, N. Sun, Y. Fang, Neuroadaptive control for complicated underactuated systems with simultaneous output and velocity constraints exerted on both actuated and unactuated states, *IEEE Trans. Neural Netw. Learn. Syst.* 34 (8) (2021) 4488–4498.
- [11] T. Yang, H. Chen, N. Sun, Y. Fang, Adaptive neural network output feedback control of uncertain underactuated systems with actuated and unactuated state constraints, *IEEE Trans. Syst. Man Cybern. Syst.* 52 (11) (2021) 7027–7043.
- [12] M.J. Maghsoudi, Z. Mohamed, S. Sudin, S. Buyamin, H. Jaafar, S. Ahmad, An improved input shaping design for an efficient sway control of a nonlinear 3D overhead crane with friction, *Mech. Syst. Signal Process.* 92 (2017) 364–378.
- [13] A.M. Abdullahi, Z. Mohamed, H. Selamat, H.R. Pota, M.Z. Abidin, F. Ismail, A. Haruna, Adaptive output-based command shaping for sway control of a 3D overhead crane with payload hoisting and wind disturbance, *Mech. Syst. Signal Process.* 98 (2018) 157–172.
- [14] N. Uchiyama, Robust control of rotary crane by partial-state feedback with integrator, *Mechatronics* 19 (8) (2009) 1294–1302.
- [15] R. Villafuerte-Segura, R. Miranda-Colorado, J.A. Rodríguez-Arellano, L.T. Aguilar, Observer-based proportional-retarded controller for payload swing attenuation of 2D-crane systems including load hoisting-lowering, *ISA Trans.* 155 (2024) 472–488.
- [16] H. Ouyang, J. Wang, G. Zhang, L. Mei, X. Deng, An LMI-based simple robust control for load sway rejection of rotary cranes with double-pendulum effect, *Math. Probl. Eng.* 2019 (2019) 1–15.
- [17] H.D. Tho, A. Kaneshige, K. Terashima, Minimum-time s-curve commands for vibration-free transportation of an overhead crane with actuator limits, *Control Eng. Pract.* 98 (2020) 104390.
- [18] J. Neupert, E. Arnold, K. Schneider, O. Sawodny, Tracking and anti-sway control for boom cranes, *Control Eng. Pract.* 18 (1) (2010) 31–44.
- [19] J. Kim, B. Kiss, D. Kim, D. Lee, Tracking control of overhead crane using output feedback with adaptive unscented Kalman filter and condition-based selective scaling, *IEEE Access* 9 (2021) 108628–108639.
- [20] C. Louembet, F. Cazaurang, A. Zolghadri, Motion planning for flat systems using positive B-splines: An LMI approach, *Automatica* 46 (8) (2010) 1305–1309.
- [21] M.S. Paing, N. Uchiyama, Spline-based time-optimal control for smooth trajectory generation of CNC machines with geometric constraints, in: 2022 IEEE 31st International Symposium on Industrial Electronics, ISIE, IEEE, 2022, pp. 1088–1093.
- [22] A. Farrage, H. Takahashi, K. Terauchi, S. Sasai, H. Sakurai, M. Okubo, N. Uchiyama, Time-optimal trajectory generation of rotary cranes with collision avoidance, *IFAC Pap.* 55 (27) (2022) 277–281.
- [23] A. Farrage, H. Takahashi, K. Terauchi, S. Sasai, H. Sakurai, M. Okubo, N. Uchiyama, Time-optimal trajectory generation of rotary cranes with load sway reduction using only horizontal boom motion, in: 2021 IEEE 30th International Symposium on Industrial Electronics, ISIE, IEEE, 2021, pp. 1–6.
- [24] N.A. Amir, H. Takahashi, A. Farrage, M.S. Paing, S. Sasai, H. Sakurai, M. Okubo, N. Uchiyama, A farrage, na amir, h takahashi, s sasai, h sakurai, m okubo, and n uchiyama, optimal trajectory generation for horizontal boom motion of rotary cranes considering load-rotation suppression, iee 3rd international conference on mechatronics, control and robotics (icmcr), pp. 113–117, 2025, *Autom. Constr.* 166 (2025) 105584.
- [25] A. Farrage, N.A. Amir, H. Takahashi, S. Sasai, H. Sakurai, M. Okubo, N. Uchiyama, Optimal trajectory generation for horizontal boom motion of rotary cranes considering load-rotation suppression, in: IEEE 3rd International Conference on Mechatronics, Control and Robotics (ICMCR), 2025, pp. 113–117.
- [26] M. Zucker, N. Ratliff, A.D. Dragan, M. Pivtoraiko, M. Klingensmith, C.M. Dellin, J.A. Bagnell, S.S. Srinivasa, Chomp: Covariant hamiltonian optimization for motion planning, *Int. J. Robot. Res.* 32 (9–10) (2013) 1164–1193.
- [27] R.T. Marler, J.S. Arora, The weighted sum method for multi-objective optimization: new insights, *Struct. Multidiscip. Optim.* 41 (2010) 853–862.
- [28] M. Diehl, H.G. Bock, H. Diedam, P.-B. Wieber, Fast direct multiple shooting algorithms for optimal robot control, *Fast Motions Biomech. Robot. Optim. Feed. Control.* (2006) 65–93.
- [29] N. Uchiyama, K. Mori, K. Terashima, T. Saeki, T. Kamigaki, H. Kawamura, Optimal motion trajectory generation and real-time trajectory modification for an industrial robot working in a rectangular space, *J. Syst. Des. Dyn.* 7 (3) (2013) 278–292.
- [30] M. Zhang, X. Ma, H. Chai, X. Rong, X. Tian, Y. Li, A novel online motion planning method for double-pendulum overhead cranes, *Nonlinear Dynam.* 85 (2016) 1079–1090.
- [31] M.N. Vu, P. Zips, A. Lobe, F. Beck, W. Kemmetmüller, A. Kugi, Fast motion planning for a laboratory 3D gantry crane in the presence of obstacles, *IFAC Pap.* 53 (2) (2020) 9508–9514.
- [32] M.N. Vu, A. Lobe, F. Beck, T. Weingartshofer, C. Hartl-Nesic, A. Kugi, Fast trajectory planning and control of a lab-scale 3D gantry crane for a moving target in an environment with obstacles, *Control Eng. Pract.* 126 (2022) 105255.

- [33] M.S. Paing, A. Farrage, N.A. Amir, H. Takahashi, K. Terauchi, S. Sasai, H. Sakurai, M. Okubo, N. Uchiyama, Real-time modification of a spline-based time-optimal motion trajectory with load-sway reduction for rotary cranes, in: 2023 9th International Conference on Control, Decision and Information Technologies, CoDIT, IEEE, 2023, pp. 1005–1010.
- [34] A. Messac, A. Ismail-Yahaya, C.A. Mattson, The normalized normal constraint method for generating the Pareto frontier, Struct. Multidiscip. Optim. 25 (2003) 86–98.
- [35] L. Biagiotti, C. Melchiorri, Trajectory Planning for Automatic Machines and Robots, Springer Science & Business Media, 2008.
- [36] P.E. Gill, E. Wong, Sequential quadratic programming methods, in: Mixed Integer Nonlinear Programming, Springer, 2011, pp. 147–224.
- [37] A. Farrage, H. Takahashi, K. Terauchi, S. Sasai, H. Sakurai, M. Okubo, N. Uchiyama, Trajectory generation of rotary cranes based on A* algorithm and time-optimization for obstacle avoidance and load-sway suppression, Mechatronics 94 (2023) 103025.
- [38] R. Siegwart, I.R. Nourbakhsh, D. Scaramuzza, Introduction to Autonomous Mobile Robots, MIT Press, 2011.